https://doi.org/10.5194/egusphere-2026-5509
Preprint. Discussion started: 29 September 2026
© Author(s) 2026. CC BY 4.0 License.

Vegetation dynamics along drydowns across global climate zones

Myriam Terristi[1,2], Sebastian Sippel[3], Benjamin D. Stocker[4,5], and Ana Bastos[1]

[1] Institute for Earth System Science and Remote Sensing, Leipzig University, Talstraße 35, 04103 Leipzig, Germany
[2] Department of Biogeochemical Signals, Max Planck Institute for Biogeochemistry, Hans-Knöll-Straße 10, 07745 Jena, Germany
[3] Institute for Meteorology, Leipzig University, Stephanstraße 3, 04103 Leipzig, Germany
[4] Institute of Geography, University of Bern, Hallerstrasse 12, 3012 Bern, Switzerland
[5] Oeschger Centre for Climate Change Research, University of Bern, Hochschulstrasse 4, 3012 Bern, Switzerland

Correspondence to: Myriam Terristi (myriam.terristi@uni-leipzig.de)

Abstract. Vegetation greenness responds dynamically to accumulating water deficits, with consequences for terrestrial carbon and water cycling. Yet how greenness changes as a deficit builds within a drydown, how this varies across climates, and how it is changing over time remain poorly resolved. Here, we analyse satellite greenness (MODIS Enhanced Vegetation Index, EVI) against cumulative water deficit (CWD, from MSWEP precipitation and GLEAM evapotranspiration) during annual maximum drydowns across the global vegetated surface from 2000 to 2023. We characterise the EVI–CWD relationship through a high-greenness peak state and a low-greenness state, separating the direction of the greenness response from its steepness. The direction of the EVI–CWD response is strongly organised by climate. Greenness tended to rise with accumulating deficit under energy limitation, covering more than half the vegetated surface, and tended to decline under water limitation. Its steepness reflected both the relative greenness change and the width of the cumulative-deficit window between the two states, so ecosystems differed both in the deficit range separating their two states and in how much greenness changed across them. Long-term trends further showed that the two states did not always change together. Peak-state EVI trends were predominantly positive across all climate-zone and regime combinations, often even where the associated CWD trend was positive. Under water limitation, however, low-state greening was consistently weaker than peak-state greening across climate zones and shifted to browning in Cold Humid regions. This contrast shows that water limitation can become more apparent at the low-greenness end of drydowns, even where peak greenness continues to rise. Resolving greenness along drydown trajectories therefore provides a more complete view of how ecosystems withstand accumulating water deficit than aggregated anomalies or single sensitivity metrics.

https://doi.org/10.5194/egusphere-2026-5509
Preprint. Discussion started: 29 September 2026
© Author(s) 2026. CC BY 4.0 License.

1 Introduction

Drought in its various forms is becoming increasingly prominent under climate change: warming raises atmospheric evaporative demand and alters precipitation regimes, increasing the frequency and severity of water deficits across many regions (IPCC, 2018, 2019, 2021). These shifts affect the hydroclimatic conditions within which terrestrial vegetation operates, increasing vegetation stress and the risk of drought-induced mortality (Brodribb et al., 2020; McDowell et al., 2008; Turner and Seidl, 2023).

Over recent decades, satellite records have shown widespread vegetation greening (Piao et al., 2019), although some studies report that greening might be levelling off as water limitation is becoming more important (Feng et al., 2021; Orth et al., 2025). Browning has also been reported across biomes, often associated with drought (Liu et al., 2021, 2023a, b), yet these long-term trends remain debated (Frankenberg et al., 2021; Jeong et al., 2024; Zhang et al., 2017). Such trends reflect not only drought but co-occurring changing drivers: elevated CO_2 and rising water-use efficiency, nutrient deposition, land-use change and management, legacies from past disturbances, and changes in land-atmosphere coupling each leave their own imprints (Bastos et al., 2020a; Liu et al., 2025; Miralles et al., 2025b; Xiao et al., 2024; Spracklen et al., 2018). Together, contrasting trends raise the question of whether and how ecosystems are responding to shifting hydroclimatic conditions, and whether apparent greening trends mask hidden vulnerabilities that emerge only as water deficits intensify.

At large scales, vegetation productivity (photosynthesis and transpiration) and the deployment of active green foliage are set by the balance between energy (temperature, radiation) and water availability, with regions differing in whether vegetation productivity is limited by one of these two components (Seneviratne et al., 2010; Nemani et al., 2003). Observationally, this control appears as a two-regime behaviour: a threshold-like dependence of photosynthesis and transpiration on soil moisture and radiation (Jonard et al., 2022). However, this balance is not stationary: a trend towards declining soil moisture along with increasing incoming solar and thermal radiation is projected to result in a long-term shift of vegetation activity from energy-limited to water-limited regimes across much of the land surface (Denissen et al., 2022), a transition characterised by a critical soil-moisture threshold beyond which water availability constrains ecosystem fluxes (Fu et al., 2022).

Individual drought events are characterised by a continuum from physical drivers to ecological impacts (Van Loon et al., 2024). Drydown events, defined as periods of progressive depletion of water available to ecosystems (McColl et al., 2017), offer a natural window onto vegetation responses under increasing water stress (Stocker et al., 2023; Fu et al., 2024). Under energy-limited conditions, such as spring in mid-latitudes, greenness may be sustained or even rise during drydown before declining once water becomes the limiting factor (Wolf et al., 2016; Bastos et al., 2020a; Buermann et al., 2018; Fig. 1b). This rise-then-decline behaviour implies a potentially non-

https://doi.org/10.5194/egusphere-2026-5509
Preprint. Discussion started: 29 September 2026
© Author(s) 2026. CC BY 4.0 License.

linear EVI–CWD response along the drydown, with the direction of the response changing as water becomes limiting. How strongly greenness declines as the water deficit accumulates, i.e., the ecosystem resistance to drought (Ingrisch and Bahn, 2018), and whether it declines at all within recorded drydown events, differ between ecosystems (Feldman et al., 2018, 2024; Jonard et al., 2022). This reflects their contrasting sensitivities to water and their spatially varying moisture thresholds (Jonard et al., 2022; Fu et al., 2022; Feldman et al., 2018, 2024), which may themselves be changing (Bastos et al., 2021). It also depends on whether the ecosystem is exposed to water limitation at all. Under relatively humid conditions, soil moisture may remain above the limitation threshold (Fu et al., 2024), while sustained access to deep soil water or groundwater can buffer vegetation against accumulating deficits, so that little water stress develops during the recorded drydowns (Giardina et al., 2023).

Greenness variations reflect changes in water availability and drought severity, as well as changes in vegetation *sensitivity* to water deficits (Bastos et al., 2023). Characterising vegetation dynamics along the energy-to-water limitation gradient, and identifying the states separating the two regimes, is therefore crucial for anticipating the impacts of a changing hydroclimate (Denissen et al., 2022).

Here, we analyse vegetation responses to drydown events from 2000 to 2023 using the Enhanced Vegetation Index (EVI), a satellite proxy for canopy greenness derived from the MODIS sensor (Didan and Munoz, 2019; Huete et al., 2002). We identify drydowns based on the Cumulative Water Deficit (CWD), and, for each drydown, analyse the dynamics of EVI to increasing CWD (Fig. 1). This allows us to characterise shifts between energy and water-limitation during drydowns across global ecosystems, identify the states corresponding to this transition, and estimate vegetation sensitivity to water stress (EVI–CWD sensitivity). Finally, we evaluate how these responses have changed during the study period. This framework addresses three scientific questions: (i) How do peak and low greenness states relate to cumulative water deficit across climate zones, and where do drydowns express energy-limited versus water-limited behaviour? (ii) How does the EVI–CWD sensitivity vary across climates, and is it controlled more by the amplitude of greenness change or by the width of the cumulative-deficit window between the two states? (iii) How have the peak and low greenness states, and their associated cumulative deficits, changed over 2000–2023, and what do their joint trends reveal about where water limitation is becoming more apparent along the drydown?

https://doi.org/10.5194/egusphere-2026-5509
Preprint. Discussion started: 29 September 2026
© Author(s) 2026. CC BY 4.0 License.

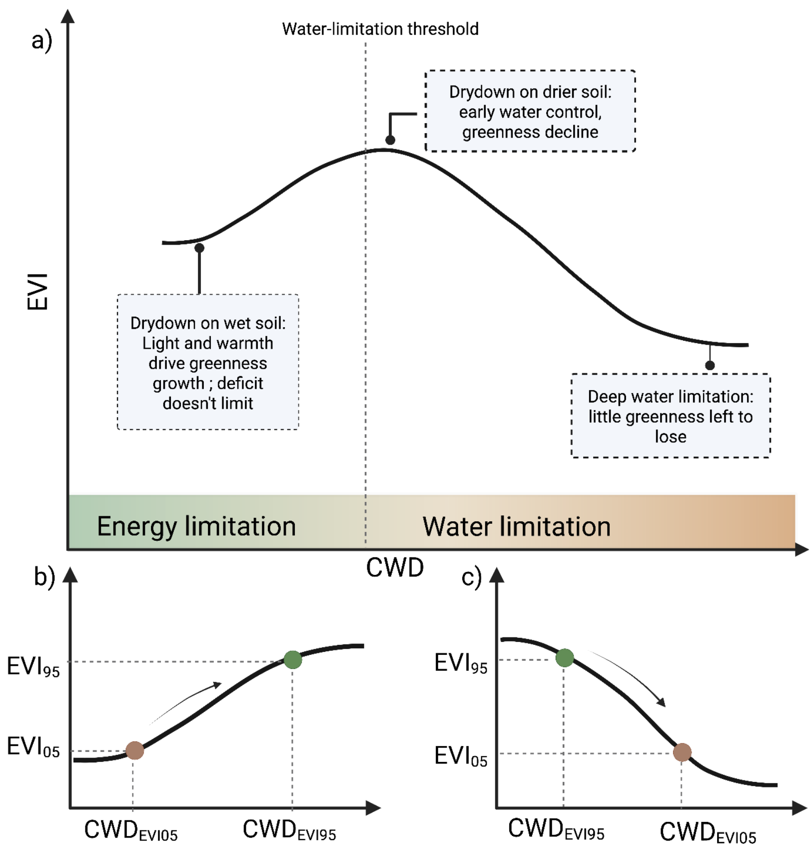

Figure 1: Drydown dynamics in the EVI–CWD space. (a) Conceptual relationship between canopy greenness (EVI) and cumulative water deficit (CWD) along a drydown draws on Feldman et al. (2024) and Feldman (2026). As the deficit accumulates (left to right), an ecosystem moves from energy-limited conditions, where light and temperature set greenness and the deficit does not yet limit it (greenness holds or rises, Fig. 1b), across the water-limitation threshold (dotted line) into water-limited conditions, where greenness declines as the deficit increases (Fig. 1c). Each grid cell is summarised by two greenness states (Sect. 2.7): (b) In the energy-limited regime the low state occurs at a lower deficit than the peak ($CWD_{EVI05} < CWD_{EVI95}$), so greenness rises as the deficit accumulates. (c) In the water-limited regime the low state occurs at a higher deficit ($CWD_{EVI05} > CWD_{EVI95}$), so greenness declines. Panels (b) and (c) are conceptual: the greenness levels are drawn at the same height in both regimes, and only the position along the CWD axis differs between them. Created in BioRender.com.

https://doi.org/10.5194/egusphere-2026-5509
Preprint. Discussion started: 29 September 2026
© Author(s) 2026. CC BY 4.0 License.

2 Data and methods

2.1 Precipitation data

Global precipitation was obtained from the Multi-Source Weighted-Ensemble Precipitation (MSWEP) dataset (V2.8; Beck et al., 2017, 2019), which combines gauge observations, satellite products, and reanalysis fields. Comparative studies have demonstrated that MSWEP outperforms many other global precipitation products, especially in remote regions (Beck et al., 2019). MSWEP v2.8 is distributed as two sub-products: a historical product, available until 2020, and a near-real-time product (NRT), which extends to the present. We used the historical product for 2000–2020 and NRT for 2021–2023 to cover the full study period. MSWEP is provided at 0.1° spatial resolution and 3-hourly time steps, which were aggregated to weekly intervals over the period 2000–2023.

2.2 Evapotranspiration data

Evapotranspiration (*ET*) was taken from GLEAM v4.2a (Miralles et al., 2025a; Miralles et al., 2011), a global daily dataset at 0.1° resolution; the product spans 1980 onward, and we use 2000–2023 to match the study period. GLEAM4 follows a hybrid framework combining a process-based water balance with a deep neural network trained on global eddy-covariance and sapflow observations to estimate evaporative stress (Koppa et al., 2022; Miralles et al., 2025a). Following GLEAM's convention, the product's variable *actual evaporation* corresponds to the sum of transpiration, interception loss, bare-soil evaporation, open-water evaporation, and snow sublimation; here we use the term 'actual evapotranspiration' (below referred to as ET) for consistency with ecohydrology terminology (Ahmad et al., 2025). In GLEAM4, potential evapotranspiration Ep is first computed using Penman's equation (Penman, 1948), explicitly accounting for wind speed, vapour pressure deficit, and vegetation height, which is used to account for canopy roughness effects on atmospheric moisture exchange. Actual evaporation E is then obtained by scaling Ep with a multiplicative evaporative-stress factor, where stress is estimated with a deep neural network that captures nonlinear controls of water limitation (e.g., soil moisture and vegetation state) and atmospheric demand (Koppa et al., 2022; Miralles et al., 2025a). The dataset was aggregated to weekly time steps.

2.3 Vegetation index data

Surface greenness was characterised using the Enhanced Vegetation Index (EVI) from the MODIS MOD13C1 Version 6.1 product, provided as 16-day composites at 0.05° (Didan and Munoz, 2019; Huete et al., 2002). EVI

https://doi.org/10.5194/egusphere-2026-5509
Preprint. Discussion started: 29 September 2026
© Author(s) 2026. CC BY 4.0 License.

was selected for its improved sensitivity in dense canopies and reduced soil and atmospheric contamination relative to NDVI (Huete et al., 2002). 16-day composites were linearly interpolated to weekly intervals to match the temporal resolution of precipitation and evapotranspiration data and spatially aggregated to 0.1° using area-weighted averaging. Weekly resolution is a practical compromise: daily precipitation and ET contain substantial short-term weather noise that is not resolved by 16-day EVI composites, while the native 16-day step can be too coarse to capture the timing of key event features.

2.4 Climate zones

Climate zones were derived from the updated Köppen–Geiger classification (V2; Beck et al., 2023) at 0.1° resolution, provided for the 1991–2020 climatological period. We grouped zones into six categories: Tropical (i), Arid Cold (ii), Temperate Dry (iii), Temperate Humid (iv), Cold Dry (v), and Cold Humid (vi). This stratification allowed us to investigate vegetation responses to hydrometeorological extremes across distinct macro-climatic environments.

2.5 Calculation of cumulative water deficit

We quantified drought severity using the cumulative water deficit (CWD), following Stocker et al. (2023). We first calculated the weekly water balance as $B_t = P_t - ET_t$, where P_t and ET_t denote precipitation and actual evapotranspiration during week t, respectively. The accumulated deficit was then expressed as a non-negative quantity:

$$CWD_t = \max(0,\ CWD_{t-1} - B_t), \tag{1}$$

where t denotes weekly time steps and $CWD_0 = 0$ at the beginning of each accumulation period.

Under this convention, CWD increases during periods of net water loss (ET > P) and decreases when precipitation exceeds actual evapotranspiration, returning to zero once precipitation has fully compensated the accumulated deficit. CWD was additionally reset to zero at the climatological wettest month to prevent multi-year accumulation in strongly seasonal climates. Individual drydown events were defined as contiguous periods of positive CWD between reset points, with each event characterised by its timing, duration, and maximum CWD. Grid cells dominated by non-vegetated land cover (urban areas, bare land, water bodies, or snow and ice) and irrigated cropland were excluded using ESA-CCI/C3S annual land-cover fractions (Copernicus Climate Change Service, Climate Data Store, 2019).

https://doi.org/10.5194/egusphere-2026-5509
Preprint. Discussion started: 29 September 2026
© Author(s) 2026. CC BY 4.0 License.

2.6 EVI dynamics during drydown events

For each grid cell and year, the annual maximum drydown event was identified as the event with the largest maximum CWD (Sect. 2.5; illustrated for an example grid cell in Fig. A1). The seasonal timing of these selected events was described by summarising their onset and end months across years for each grid cell using the circular median (Fig. A2). For the EVI–CWD analysis, all weekly (CWD, EVI) observations from these annual maximum drydowns across the study period (2000–2023) were pooled. The pooled observations were then summarised by two contrasting dynamical states. The peak state represents the grid cell at its highest greenness: EVI_{95} is defined as the median of the highest 5 % of the pooled EVI values, and CWD_{EVI95} as the corresponding median CWD of those same observations. The low state represents the grid cell at its lowest greenness: EVI_{05} is the median of the lowest 5 % of the pooled EVI values, and CWD_{EVI05} is the median CWD of those observations.

The two states are distinguished by a relative greenness amplitude and a cumulative-deficit distance. The cumulative-deficit distance was defined as $\Delta CWD = |CWD_{EVI05} - CWD_{EVI95}|$. The relative position of the two states along the deficit axis determines each grid cell's drydown regime: when the low state occurs at a higher deficit than the peak ($CWD_{EVI05} > CWD_{EVI95}$), greenness declines as the deficit accumulates, indicating a water-limited regime (Fig. 1c). Conversely, when the low state occurs at a lower deficit than the peak ($CWD_{EVI05} < CWD_{EVI95}$), greenness increases as the deficit accumulates, indicating an energy-limited regime (Fig. 1b). This peak-to-low comparison provides an empirical, greenness-based classification of the limitation regime each grid cell expresses during its drydowns, and we use this pooled characterisation to compare regimes across climate zones. For the trend analysis (Sects. 2.8–2.9), the two states were instead computed annually, resulting in a time series of EVI_{95}, CWD_{EVI95}, EVI_{05}, and CWD_{EVI05} for each grid cell.

2.7 EVI–CWD sensitivity

To quantify how greenness varies with accumulating water deficit, we define the EVI–CWD sensitivity of each grid cell as the signed relative greenness change between the two states per unit of cumulative deficit separating them. Because EVI_{05} is by definition lower than EVI_{95}, the magnitude of the relative greenness change was first computed as: $|\Delta EVI| = 100 \times (EVI_{95} - EVI_{05}) / EVI_{95}$. This amplitude is always positive.

Its sign was then assigned according to the relative position of the two states along the CWD axis: (i) $\Delta EVI = +|\Delta EVI|$ when $CWD_{EVI05} < CWD_{EVI95}$, indicating an energy-limited regime in which greenness increases as the deficit accumulates; and (ii) $\Delta EVI = -|\Delta EVI|$ when $CWD_{EVI05} > CWD_{EVI95}$, indicating a water-limited regime in which greenness declines as the deficit accumulates. The cumulative water deficit distance was defined as: $\Delta CWD = |CWD_{EVI05} - CWD_{EVI95}|$. The EVI–CWD sensitivity was then calculated as:

https://doi.org/10.5194/egusphere-2026-5509
Preprint. Discussion started: 29 September 2026
© Author(s) 2026. CC BY 4.0 License.

$$Sensitivity = \frac{\Delta EVI}{\Delta CWD} \quad (2)$$

expressed in % mm^{-1}. Negative sensitivity values indicate greenness decline with accumulating deficit in water-limited drydowns, whereas positive values indicate greenness increase with accumulating deficit in energy-limited drydowns. The sign of the sensitivity therefore distinguishes the two regimes, while its magnitude indicates the steepness of the EVI–CWD relationship in both cases.

2.8 Trend detection for CWD and EVI states

For the trend analysis, the two states were extracted per year rather than from the pooled distribution. For each grid cell and year, EVI_{95}, CWD_{EVI95}, EVI_{05}, and CWD_{EVI05} were taken from the annual maximum drydown event (Sect. 2.6), yielding an annual time series of the four states from 2000 to 2023 for each grid cell. We tested each series for a monotonic temporal trend using the Mann–Kendall test (Kendall, 1975; Mann, 1945), implemented in the Kendall R package (McLeod, 2005). We estimated the trend magnitude with the Theil–Sen slope using the trend R package (Pohlert, 2015), reported as change per decade. Because hydroclimate and vegetation time series can exhibit positive autocorrelation that may inflate nominal significance, we used annual, event-based aggregates to limit short-memory effects. We report the Sen slope alongside p-values so that significance and effect size are evaluated jointly. Differences in Sen-slope distributions across climate zones were assessed with a Kruskal–Wallis test followed by pairwise Wilcoxon rank-sum tests.

2.9 Joint EVI–CWD trend trajectories

Building on the per-metric trend analysis (Sect. 2.8), we summarised the joint changes in greenness and water deficit at each state. For each climate zone, state (peak, low), and regime, grid cells were mapped in a bivariate space defined by their per-decade Sen slopes (CWD slope on the x-axis, EVI slope on the y-axis). The bivariate distribution for each group was estimated using a two-dimensional kernel density estimator (MASS R package; Venables and Ripley, 2002). The two-dimensional mode, defined as the location of maximum density, was extracted from each distribution to summarise the dominant trend direction. Groups with fewer than 10 grid cells were not assigned a mode. The displacement from the peak-state mode to the low-state mode is represented as an arrow (Fig. 5). We then classified grid cells into four trajectories according to the sign of their EVI and CWD trends: (i) Greening–Drying (GD), positive EVI and positive CWD; (ii) Greening–Attenuating (GA), positive EVI and negative CWD; (iii) Browning–Drying (BD), negative EVI and positive CWD; and (iv) Browning–Attenuating (BA), negative EVI and negative CWD.

https://doi.org/10.5194/egusphere-2026-5509
Preprint. Discussion started: 29 September 2026
© Author(s) 2026. CC BY 4.0 License.

2.10 Statistical testing

Our analyses compare distributions across the global vegetated land surface, so group sizes are very large (tens of thousands to several hundred thousand grid cells per climate zone; Table A1). At such sample sizes, significance testing is limited: even negligible differences become statistically significant, so p-values indicate only that a difference exists, not whether it is meaningful (Lin et al., 2013; Nakagawa and Cuthill, 2007). We therefore summarise distributions non-parametrically and quantify differences between EL–WL regimes and climate zones with effect sizes, which are largely independent of sample size, rather than only relying on p-values. Each variable was summarised per climate zone and drydown regime. Because the distributions were strongly skewed, we described them by medians and interquartile ranges (IQRs) rather than means and standard deviations; the per-zone medians, IQRs and skewness values are reported in Appendix A.

Differences among the six climate zones were assessed with the Kruskal–Wallis test (Kruskal and Wallis, 1952), the rank-based analogue of a one-way ANOVA, which makes no assumption of normality and so suits our skewed data. The strength of the zone effect was quantified by the epsilon-squared effect size (ε^2), which rescales the Kruskal–Wallis statistic to a 0–1 range and estimates the proportion of the rank variance attributable to climate zone (0 = zones do not separate, 1 = zones separate completely; Tomczak and Tomczak, 2014). Pairwise differences between zones were quantified with Cliff's delta (Cliff, 1993), a non-parametric effect size equal to the difference between the probability that a randomly drawn value from one zone exceeds a value drawn from another and the reverse probability. Cliff's delta ranges from −1 to +1, where 0 indicates complete overlap of the two distributions and ±1 indicates no overlap; its magnitude was interpreted following Romano et al. (2006) as negligible ($|\delta| < 0.147$), small ($0.147 \leq |\delta| < 0.330$), medium ($0.330 \leq |\delta| < 0.474$) or large ($|\delta| \geq 0.474$).

3 Results

3.1 Drydown regimes and greenness states

The drydown regime during the study period (2000–2023) is strongly explained by background climate conditions (Fig. 2g). Energy-limited drydowns were found predominantly in cold zones (87 % of Cold Humid and Cold Dry grid cells and 59 % of Arid Cold), whereas water-limited drydowns prevailed in the Temperate Dry (80 %) and Tropical (67 %) zones (Fig. 2g; area-weighted per-zone fractions and n in Table A1). Across all zones, ~ 56 % of the vegetated surface was mainly energy-limited (area-weighted), including the boreal and temperate north and the humid tropics. The remaining vegetated surface (44 %) was mainly water-limited, including drylands, the Mediterranean, and the seasonally dry tropics.

https://doi.org/10.5194/egusphere-2026-5509
Preprint. Discussion started: 29 September 2026
© Author(s) 2026. CC BY 4.0 License.

By definition, the EVI response to drydowns (ΔEVI) is positive on average for energy-limited regimes, and negative for water-limited regimes, but we found considerable differences across climate zones (Fig. 2a–c, Table A2). The median response was smallest in the humid and tropical zones (a water-limited loss of ~52 % in the Tropics and 54 % in Temperate Humid, and an energy-limited gain of ~30 % in the Tropics) and the largest in the arid and cold zones (water-limited losses of ~77–88 %; energy-limited gains up to ~94 %). Climate zone explained a large share of the variation in ΔEVI in both regimes, more so under energy limitation, meaning that where a pixel sits climatically shapes how much its greenness changes during drydown, beyond its regime alone (Kruskal–Wallis $\varepsilon^2 = 0.35$ water-limited, 0.45 energy-limited; all $p < 0.001$; Table A3). The contrast was clearest between the Tropics and Cold Dry, which barely overlap in either regime (Cliff's $|\delta| = 0.78$ water-limited, 0.97 energy-limited; Table A4).

The magnitude of the drydown between the 5th and 95th percentiles of EVI (ΔCWD) also varied widely between zones in both regimes (Fig. 2f, Table A2; global maps in Fig. A3a–b). ΔCWD differences across regions span a magnitude of about six-fold in water-limited grid cells (median ~14 mm in Cold Humid to ~83 mm in Temperate Dry) and about three-fold in energy-limited grid cells (~16 mm in Arid Cold to ~45 mm in the Tropics), with strongly right-skewed distributions. In the water-limited regime the widest deficit spans (Tropics and Temperate Dry, ~81–83 mm) fell in the zones with the smallest greenness losses, and the narrowest (cold and arid, ~14–28 mm) where losses were the largest (Fig. 2c,f). The zone effect on ΔCWD was strong in the water-limited regime ($\varepsilon^2 = 0.24$; largest contrast Temperate Dry vs Cold Humid, Cliff's $\delta = 0.73$) but weak in the energy-limited regime ($\varepsilon^2 = 0.10$; all $p < 0.001$; Tables A3 and A4).

Within a given climate zone, we found similar values of EVI_{05} and EVI_{95} for the two regimes (|Cliff's δ| < 0.3; Table A5); the clearest exception was the Tropics, where energy-limited pixels were greener than water-limited pixels, most markedly at their low-greenness state (median $EVI_{05} \sim 0.42$ vs ~ 0.22, $\delta = 0.49$) but also at their peak ($EVI_{95} \sim 0.60$ vs ~ 0.51, $\delta = 0.48$; Fig. 2a,b). A higher energy-limited peak was also found in Cold Dry ($\delta = 0.47$). The CWD at which peak greenness was reached (CWD_{EVI95}; Fig. 2d) differed markedly between regimes in the Tropics: approximately 127 mm in energy-limited pixels versus 40 mm in water-limited pixels.

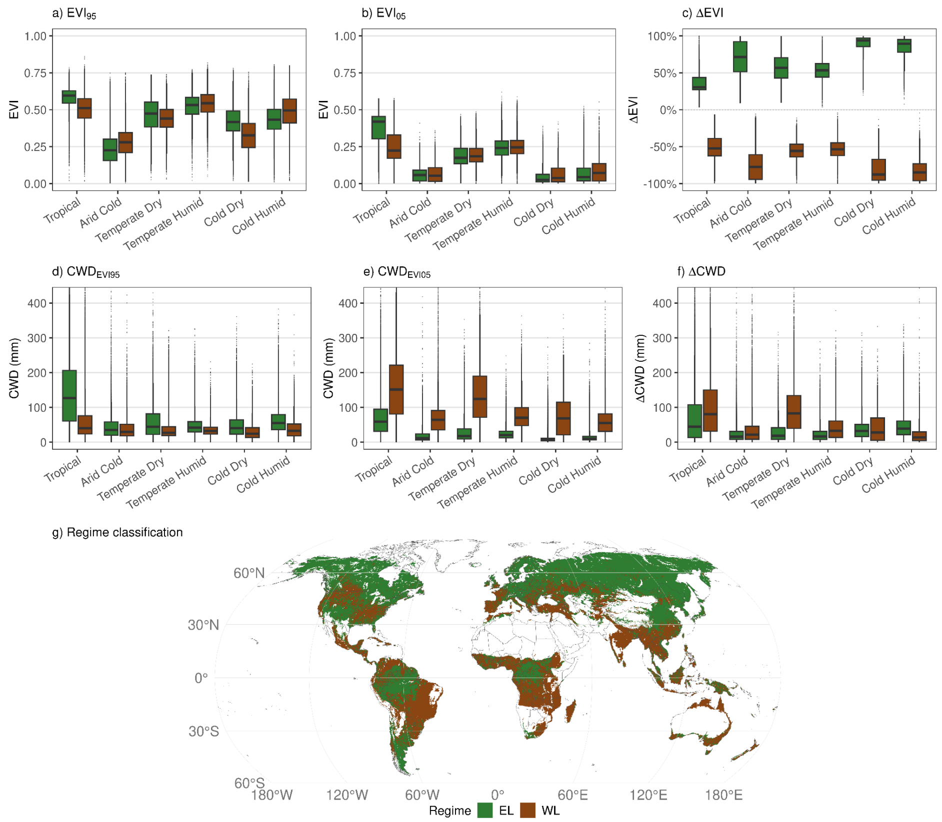

Figure 2: Greenness and cumulative water deficit at the peak and low states across climate zones for the two regimes. (a) EVI_{95} and (b) EVI_{05}, the greenness at the peak and low states; (c) ΔEVI, the relative greenness change between the two states, signed by regime (see Sects. 2.6–2.7); (d) CWD_{EVI95} and (e) CWD_{EVI05}; (f) ΔCWD, the deficit distance between the two states. Boxes show the median and interquartile range by climate zone and drydown regime (energy-limited, green; water-limited, brown); whiskers extend to 1.5 × IQR and outliers are shown as points. Boxplots show distribution of grid-cell values pooled from the annual-maximum drydowns over 2000–2023. (g) Global drydown-regime classification. Statistics per climate zone are given in Tables A1–A5.

3.2 Vegetation sensitivity to drought

EVI–CWD sensitivity (Sect. 2.7) varied between climate zones in both regimes, though more so under water limitation (Fig. 3, Table A6; Kruskal–Wallis $\varepsilon^2 = 0.31$ water-limited vs 0.14 energy-limited, Table A7).

In the water-limited regime, EVI–CWD sensitivity was most negative, i.e., greenness declining most steeply per mm of deficit, in the cold and arid zones (median −3.9 % mm^{-1} in Cold Humid and −2.7 % mm^{-1} in Arid Cold), and less negative, and comparable to each other, in the dry-temperate and tropical zones (both about −0.6 % mm^{-1}; Cliff's $\delta = -0.08$, negligible; Table A8). The distributions were left-skewed with heavy lower tails: the 5^{th} percentile reached about −14 % mm^{-1} in Cold Humid and −12 to −13 % mm^{-1} in the other cold and arid zones

https://doi.org/10.5194/egusphere-2026-5509
Preprint. Discussion started: 29 September 2026
© Author(s) 2026. CC BY 4.0 License.

(Table A6). The largest difference was between the most and least sensitive zones (Cold Humid vs Tropical, Cliff's |δ| = 0.82; Table A8).

Under energy limitation, a broadly mirrored pattern emerged with the opposite sign: EVI–CWD sensitivity was clearly lowest in the Tropics (median +0.6 % mm^{-1}) and higher, but comparable among themselves, across the other five zones (medians ~2.1–3.5 % mm^{-1}; pairwise |Cliff's δ| < 0.15 for most zone pairs, Table A9), with Arid Cold marginally the steepest (+3.5 % mm^{-1}). As in the water-limited regime, the distributions were right-skewed with heavy tails, here on the positive side, with the 95th percentile reaching about +12 % mm^{-1} in Arid Cold and +11 % mm^{-1} in Cold Dry, versus about +7 % mm^{-1} in the Tropics (Table A6). The climate-zone effect was weaker than under water limitation (ε^2 = 0.14 vs 0.31), and the only robust contrast was between the Tropics and the other zones (e.g. Arid Cold vs Tropical, δ = 0.68; Table A9).

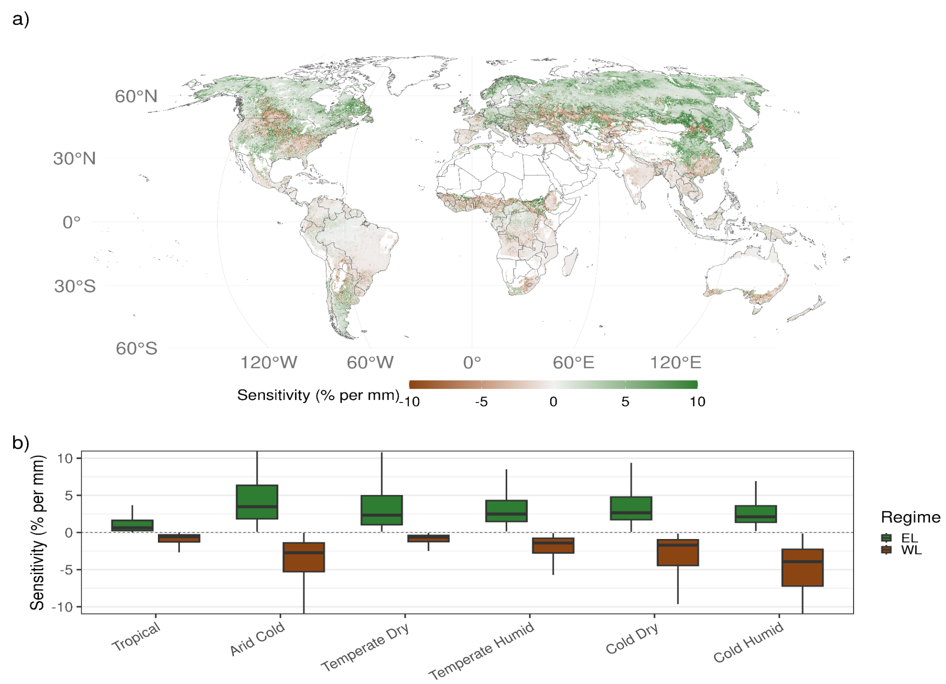

Figure 3: Vegetation sensitivity to drought (Sensitivity, % mm^{-1}) across climate zones. (a) Global map of EVI–CWD sensitivity on a diverging scale from brown (water-limited, Sensitivity < 0), pale grey (Sensitivity ~ 0) to green (energy-limited, Sensitivity > 0). The colour scale is capped at ±10 % mm^{-1}; (b) Distribution of Sensitivity by climate zone and drydown regime (energy-limited, green; water-limited, brown); boxes show the median and interquartile range, whiskers 1.5 × IQR, outliers not shown, on the same ±10 % mm^{-1} scale as (a). Sensitivity is defined in Sect. 2.7; per-zone medians, spread and effect sizes (Kruskal–Wallis ε^2, pairwise Cliff's δ) are given in Tables A6–A9.

https://doi.org/10.5194/egusphere-2026-5509
Preprint. Discussion started: 29 September 2026
© Author(s) 2026. CC BY 4.0 License.

3.3 EVI trends for the peak and low states

To characterise long-term change, we first mapped the sign of the EVI trends at the peak (EVI_{95}) and low (EVI_{05}) greenness states over 2000–2023, classifying each grid cell by the combination of the two signs (Fig. 4; absolute trend values in Fig. A4; significance in Fig. A5).

In both regimes, the most common combination was greening at both states ($EVI_{95}\uparrow/EVI_{05}\uparrow$, Fig. 4). This class covered 47 % of energy-limited and 48 % of water-limited grid cells after area weighting and was the most frequent class in every climate zone, ranging from 39 % to 60 % (Tables A10 and A11). It was most frequent in Temperate Dry regions, where it represented 57 % of energy-limited and 60 % of water-limited grid cells. Under energy limitation, it also represented 52 % of grid cells in both Cold Dry and Tropical regions, while under water limitation it represented 47 % and 53 %, respectively.

Despite this overall greening tendency, the peak and low states frequently changed in opposite directions. Opposing trend signs occurred in 39 % of energy-limited and 37 % of water-limited grid cells. Under energy limitation, the most frequent divergent combination was peak-state greening with low-state browning ($EVI_{95}\uparrow/EVI_{05}\downarrow$), which represented 24 % of grid cells, compared with 21 % under water limitation. This class was particularly frequent in the energy-limited Cold Humid and Cold Dry zones, where it represented 30 % and 25 % of grid cells, respectively (Table A11).

The latitudinal profiles further show that the two classes involving low-state browning were concentrated at northern high latitudes (Fig. 4, side panels). Peak-state greening combined with low-state browning was the more frequent of these classes across the Cold Humid and Cold Dry zones, while double browning showed an additional high-latitude concentration. The opposite divergent combination, peak-state browning with low-state greening ($EVI_{95}\downarrow/EVI_{05}\uparrow$), was slightly more frequent under water limitation than under energy limitation, representing 17 % and 15 % of grid cells, respectively.

Browning at both states ($EVI_{95}\downarrow/EVI_{05}\downarrow$) had a similar overall prevalence in the two regimes, representing 15 % of water-limited and 14 % of energy-limited grid cells. Under energy limitation, this class occurred mainly across northern Eurasia, Canada and parts of western Europe, whereas under water limitation it was visible across regions including California, the southeastern United States and central Europe (Fig. 4).

A significant trend in at least one greenness state (Mann–Kendall $p < 0.05$) was detected in 28 % of energy-limited and 27 % of water-limited grid cells (Fig. A5). The four trend combinations remained represented when the analysis was restricted to this significant subset, although their relative frequencies changed (Table A10).

https://doi.org/10.5194/egusphere-2026-5509
Preprint. Discussion started: 29 September 2026
© Author(s) 2026. CC BY 4.0 License.

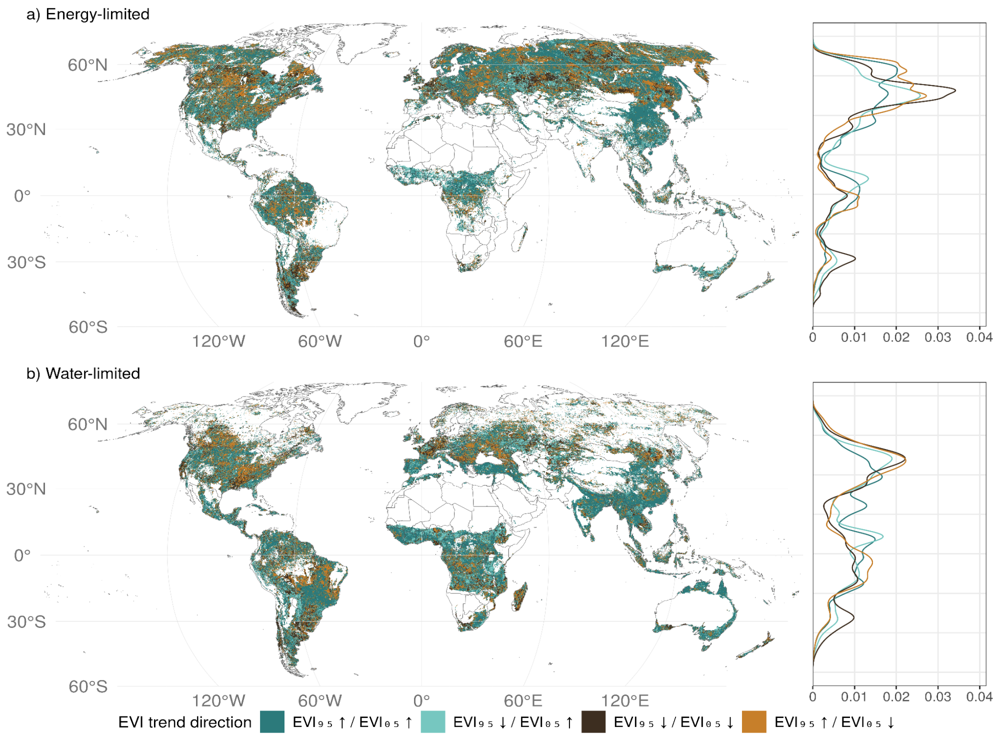

Figure 4: Direction of EVI trends at the peak and low greenness states, 2000–2023. Each grid cell is classified by the combined sign of the Theil–Sen trends in peak greenness (EVI_{95}) and low greenness (EVI_{05}), for (a) energy-limited and (b) water-limited grid cells. Colours denote the four sign combinations (legend); grid cells with no detectable trend in either state are not shown. Side panels show the area-weighted latitudinal density of each class. All classified pixels are displayed regardless of significance; the corresponding Mann–Kendall p-values are mapped in Fig. A5, and per-class fractions (all pixels and significant subset) are given in Table A10.

3.4 Coupling of vegetation greenness and water deficit trends

We then evaluated whether the EVI trends at each state coincided with trends in the associated cumulative water deficit (Fig. 5; Sect. 2.9). Across the 24 state × climate-zone × regime distributions, 23 modes were located in the greening half of the EVI–CWD trend space (Fig. 5; Table A12). The only exception was the water-limited Cold Humid zone, where the peak-state mode was located in greening–drying and the low-state mode in browning–drying.

In the energy-limited regime, the modes of both states were located in the greening half of the trend space in every climate zone. Within each state × climate-zone group, 65–92 % of grid cells had positive EVI trends (n = 243–6,593 per group; Tables A12 and A13). Outside the temperate zones, the peak- and low-state EVI modes differed by no more than 0.011 per decade, indicating that their separation occurred mainly along the CWD-trend axis.

https://doi.org/10.5194/egusphere-2026-5509
Preprint. Discussion started: 29 September 2026
© Author(s) 2026. CC BY 4.0 License.

The separation was larger in Temperate Dry and Temperate Humid, where the low-state EVI mode was respectively 0.040 per decade lower and 0.033 per decade higher than the peak-state mode.

The low-state mode was located in the greening–drying quadrant in all six energy-limited climate zones, with CWD trends ranging from +3.6 mm per decade in Cold Dry to +33.6 mm per decade in the Tropics. The peak-state mode was located in greening–drying in the Tropical, Cold Dry and Cold Humid zones, and in greening–attenuating in Arid Cold, Temperate Dry and Temperate Humid. In Temperate Humid, for example, the peak-state mode was located in greening–attenuating (CWD −52.9 mm per decade, EVI +0.035 per decade), whereas the low-state mode was located in greening–drying (CWD +11.1 mm per decade, EVI +0.068 per decade).

In the water-limited regime, the peak-state mode was located in the greening half of the trend space in every climate zone, with EVI trends ranging from +0.011 per decade in Arid Cold to +0.069 per decade in Cold Humid. Across zones, 71–87 % of grid cells had positive peak-state EVI trends (Table A13). The peak-state mode was located in greening–drying in four zones and in greening–attenuating in Arid Cold and Cold Dry.

In contrast to the energy-limited regime, the low-state EVI mode was lower than the peak-state mode in all six water-limited climate zones. This contrast was largest in Cold Humid, where the peak-state mode was located in greening–drying (CWD +40.5 mm per decade, EVI +0.069 per decade) and the low-state mode in browning–drying (CWD +87.4 mm per decade, EVI −0.069 per decade). This was the largest difference between the peak- and low-state EVI modes across all climate-zone and regime combinations. In this group, 43 % of low-state grid cells were classified as browning–drying, while 50 % retained a positive EVI trend (Table A13).

In Temperate Humid, the water-limited low-state KDE was bimodal, with one lobe in greening–attenuating and another in browning–drying; 41 % and 37 % of grid cells fell in these two quadrants, respectively, while the peak-state mode was located in greening–drying (Fig. 5; Table A13). In the remaining water-limited zones, the low-state EVI modes remained positive but small. Their CWD modes were negative in the Tropical, Arid Cold and Temperate Dry zones and positive in Cold Dry (Table A12).

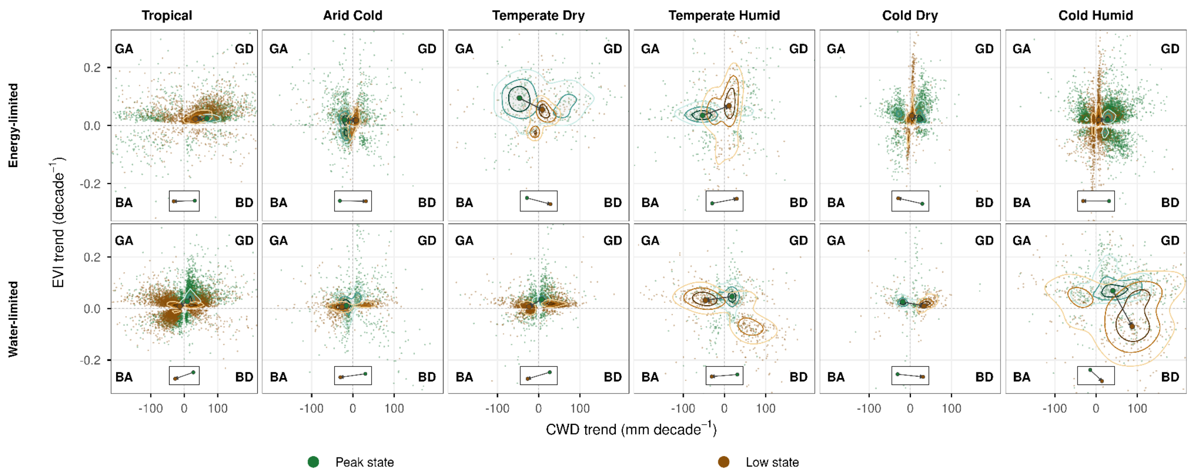

Figure 5: Joint EVI–CWD trend trajectories at the peak and low greenness states. Bivariate kernel density estimates (KDEs) of per-decade trends in canopy greenness (EVI trend, y-axis, per decade) and cumulative water deficit (CWD trend, x-axis, mm per decade), for each climate zone (columns) and drydown regime (rows). Within each panel the two greenness states are shown separately, the peak state (green) and the low state (brown). The coloured lines show the KDE contours of each state, and the filled dot marks the two-dimensional mode (the highest-density trend) of each state. The black arrow runs from the peak-state mode to the low-state mode. Dashed grey lines at zero divide the space into four trajectory quadrants, labelled by the sign of the EVI and CWD trends (see Sect. 2.9). Only grid cells with significant EVI or CWD trend are shown; sample sizes per state × zone × regime are given in Table A12.

3.5 Regime shifts during extreme years

We next examined whether the climatological drydown regime persisted during years associated with extreme droughts in some of the energy-limited regions identified above, namely 2010 (Amazon and western Russia), 2015 (tropics and southern Europe) and 2018 (western and northern Europe). Temporary shifts from energy-limited to water-limited behaviour occurred across a broad range of regions in all three selected years (Fig. 6). After area weighting, 22.5 % of the climatologically energy-limited area expressed water-limited behaviour in 2010, 23.5 % in 2015 and 22.5 % in 2018. The global fractions were therefore similar across years. Spatial concentrations of shifts were recurrent across North America, Eurasia and tropical regions in all three years. Their relative prominence varied among years. Western Russia was more visible in 2010, while central Europe appeared in both 2015 and 2018. Parts of the Amazon and Southeast Asia were also visible in 2015, whereas a broader concentration across East Asia was apparent in 2018. The fraction of climatologically energy-limited cells switching to water-limited behaviour also varied among climate zones (Table A14). It reached up to 48 % in Temperate Dry and 46 % in Temperate Humid regions in at least one of the selected years, compared with 12–19 % in the cold zones. Extending the analysis to all years (2000–2023), the area of climatologically energy-limited

https://doi.org/10.5194/egusphere-2026-5509
Preprint. Discussion started: 29 September 2026
© Author(s) 2026. CC BY 4.0 License.

ecosystems expressing water-limited behaviour varied from year to year without a clear directional change (Fig. A6).

https://doi.org/10.5194/egusphere-2026-5509
Preprint. Discussion started: 29 September 2026
© Author(s) 2026. CC BY 4.0 License.

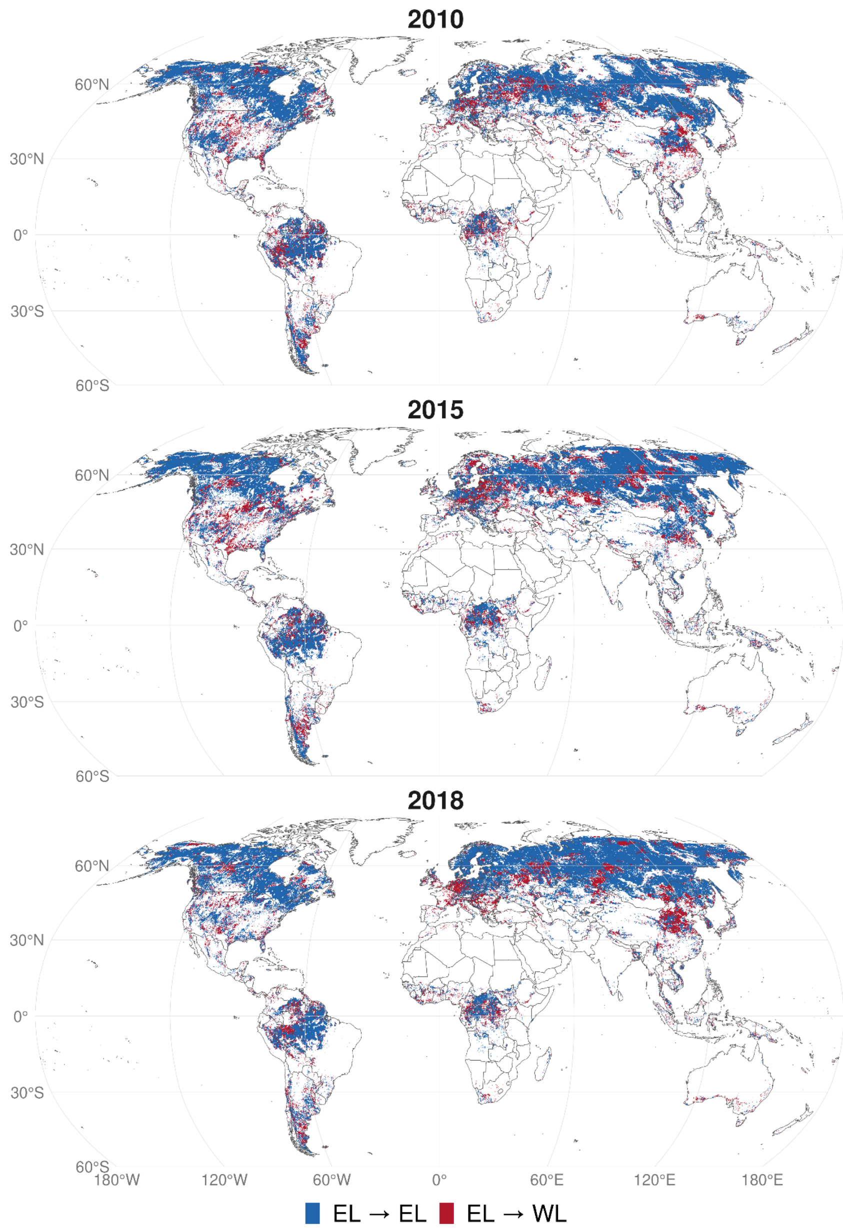

395

https://doi.org/10.5194/egusphere-2026-5509
Preprint. Discussion started: 29 September 2026
© Author(s) 2026. CC BY 4.0 License.

Figure 6: Shifts from energy-limited to water-limited behaviour during selected extreme years. For grid cells classified as energy-limited from the pooled 2000–2023 drydowns, the maps show whether the annual maximum drydown remained energy-limited (blue) or expressed water-limited behaviour (red) in (a) 2010, (b) 2015 and (c) 2018. Water-limited behaviour was identified when the low-greenness state occurred at a higher cumulative water deficit than the peak state ($CWD_{EVI05} > CWD_{EVI95}$). White areas indicate grid cells that were climatologically water-limited, excluded from the analysis.

4 Discussion

4.1 A dynamic perspective on responses to drought

Here we find that the direction and steepness of vegetation greenness change along drydowns provide complementary information. The relative position of the peak and low states identifies the predominant EVI–CWD regime expressed across the pooled annual maximum drydowns, whereas EVI–CWD sensitivity quantifies the greenness difference between those states per unit cumulative deficit. This classification summarises the predominant drydown behaviour over 2000–2023 and does not imply that greenness increases with drought in every event or that water limitation is absent. Indeed, some grid cells classified as predominantly energy-limited expressed water-limited behaviour during individual extreme years (Fig. 6).

Studies have quantified drought impacts using seasonal or annual anomalies in vegetation activity, either by focusing on individual extreme events (Ciais et al., 2005; Bastos et al., 2020b; Wolf et al., 2016; Anderegg et al., 2020), or through spatially aggregated sensitivity metrics across pixels, ecosystems or biomes (Vicente-Serrano et al., 2013; Seddon et al., 2016). A complementary line of research has analysed drydowns as transitions between energy- and water-limited states, particularly to partition evaporation regimes and identify critical soil-moisture thresholds (Akbar et al., 2018; Feldman et al., 2019; Fu et al., 2022).

Building on this dynamic perspective, we track EVI along a continuum of increasing cumulative water deficit during annual maximum drydowns over the 24-year period 2000–2023. Rather than quantifying aggregated vegetation anomalies over a predefined drought period, we evaluate how greenness changes along the drydown trajectory. Because this event-relative framing is anchored to each event's own accumulating deficit rather than to a fixed calendar period, it also avoids the prior de-seasonalisation of the greenness signal that anomaly-based metrics require. This addresses a recurring challenge in drought–vegetation studies: drought may be defined either from the physical water deficit perspective or from its observed ecological impact, and these definitions do not necessarily identify the same events (Slette et al., 2019; Flach et al., 2018). By relating EVI directly to cumulative water deficit within each drydown event, our framework characterises the direction and steepness of the greenness response without imposing a predefined sign or magnitude. It therefore distinguishes drydowns in which the peak-

https://doi.org/10.5194/egusphere-2026-5509
Preprint. Discussion started: 29 September 2026
© Author(s) 2026. CC BY 4.0 License.

greenness state occurs at a higher cumulative deficit from those in which the low-greenness state occurs at a higher cumulative deficit. This distinction is motivated by the potentially non-linear EVI–CWD response illustrated in Fig. 1. Greenness may initially increase while energy remains limiting, reach a peak, and then decline once water limitation develops. Our two-state framework does not reconstruct the full response curve or identify its turning point. Instead, it determines whether the relative ordering of the peak and low states is consistent with the increasing or declining part of such a response.

At the pooled 2000–2023 scale, the two regimes occupied broadly comparable shares of the global vegetated surface but were distributed differently among climate zones. Cold Dry and Cold Humid regions were predominantly energy-limited, whereas Tropical and Temperate Dry regions were predominantly water-limited (Fig. 2g; Table A1). This spatial organisation is consistent with broad climatic controls on vegetation activity through the balance between energy and water availability (Nemani et al., 2003; Jiao et al., 2021; Seneviratne et al., 2010). However, a predominantly energy-limited classification does not exclude a later transition to water limitation once a higher deficit is reached, and our two-state framework does not identify the CWD threshold at which such a transition occurs.

The timing of drydown onset also matters for interpreting positive EVI–CWD relationships. In the cold zones, annual maximum drydowns often began during spring and extended into summer or early autumn (Fig. A2). Increasing EVI and CWD may therefore partly reflect concurrent canopy development and deficit accumulation rather than a beneficial effect of water deficit. This helps to interpret earlier reports of positive vegetation responses during soil-moisture droughts or warm and dry anomalies, which have been linked to energy limitation, spring phenology and seasonal compensation (Walther et al., 2016; Bastos et al., 2020b; Miller et al., 2023; Buermann et al., 2018; Flach et al., 2018).

4.2 The deficit window modulates EVI–CWD sensitivity

Within most climate zones, peak-state greenness was broadly similar between energy- and water-limited regimes, even though the peak and low states occurred at different positions along the cumulative-deficit axis (Fig. 2; Table A5). This pattern suggests that background climate and vegetation characteristics constrain the greenness level reached at the peak state, whereas the regime distinction is expressed more clearly through the CWD associated with the two states. Cross-regime differences in peak-state EVI were largest in the Tropical and Cold Dry zones (Fig. 2), and smaller elsewhere.

EVI–CWD sensitivity integrates two dimensions of the drydown response: the relative greenness difference between the peak and low states and the cumulative-deficit distance separating them. For a given greenness

https://doi.org/10.5194/egusphere-2026-5509
Preprint. Discussion started: 29 September 2026
© Author(s) 2026. CC BY 4.0 License.

contrast, a narrower deficit window produces a larger absolute sensitivity, whereas a broader window produces a shallower response. EVI–CWD sensitivity should therefore be interpreted jointly in terms of its magnitude and the prevailing regime. Large negative values indicate a rapid loss of greenness per unit cumulative deficit, whereas large positive values indicate a rapid increase in greenness over the observed deficit window. Positive sensitivity should not, however, be interpreted as evidence that increasing water deficit benefits vegetation.

This distinction is particularly important in cold and high-latitude regions. In Cold Humid regions, the median onset of annual-maximum drydowns was concentrated in April and May, with median end dates extending through summer and into early autumn; Cold Dry drydowns also tended to begin during spring (Fig. A2). CWD accumulation can therefore coincide with spring leaf-out and rapid canopy development. Snow storage and snowmelt, which are not represented explicitly in the CWD calculation, may also affect the timing of deficit onset and the satellite greenness signal (Jeong et al., 2011, 2017; Wang et al., 2017; Cao et al., 2020). Steep positive sensitivities in these regions may therefore partly reflect seasonal covariation between canopy development and CWD accumulation, whereas steep negative sensitivities describe rapid greenness loss over a narrow deficit interval. Neither directly quantifies physiological plant water stress.

The strongest combined contrast between regimes across both greenness states occurred in the Tropics. Tropical energy-limited grid cells had higher median EVI than water-limited grid cells at both the peak and low states and reached peak greenness at a higher cumulative deficit, although the Tropical zone as a whole was predominantly water-limited (Fig. 2; Tables A1 and A5). Cold Dry also showed a clear cross-regime difference at the peak state. These patterns indicate substantial heterogeneity within climate zones. Differences in vegetation structure, rooting depth and access to stored water provide plausible explanations, particularly because deep-rooted tropical vegetation may maintain canopy activity through access to deeper water reserves (Chitra-Tarak et al., 2021; Christina et al., 2017; Kühnhammer et al., 2023).

The varying deficit range is consistent with other drydown studies showing that plant water-stress thresholds and rooting-zone water storage vary with background hydroclimate. Fu et al. (2024), for example, showed that critical soil-moisture thresholds differ between arid and humid ecosystems, while Stocker et al. (2023) showed that rooting-zone water-storage capacity varies widely across the global vegetated land surface. Our study is consistent with those results, but we further quantify the corresponding gain or decline in EVI. When controlling for regional differences in the vegetation cover, we find a remarkable consistency of relative EVI gain or decline across climate zones.

© Author(s) 2026. CC BY 4.0 License.

4.3 Peak and low greenness changed differently over time

We find that, in spite of drying trends in many regions, greening remained the dominant signal at the peak state in both energy-limited and water-limited systems (Figs. 4 and 5). In energy-limited regimes, greening predominated at both the peak and low states; in water-limited systems in many regions, however, the low state showed slower greening than the peak or even browning (Fig. 5). Our event-based EVI–CWD analysis thus helps to reconcile reports of global greening (Zhu et al., 2016; Piao et al., 2019) with studies showing an increase in browning trends along with increasing drought (Pan et al., 2018; Jiao et al., 2021). When considering trends in the drydown dynamics, we show that long-term change is not simply a division between greening and browning regions, but rather a widening of the difference between peak and low greenness, especially in water-limited systems (Figs. 4 and 5). This widening is consistent with the idea that the two drydown states are increasingly shaped by different dominant controls. At the peak state, greenness increased in every climate zone and independently of the corresponding CWD trend. This pattern is consistent with a predominant role for other global greening drivers, such as CO_2 fertilisation, warming and land-use change, and may also indicate that higher water-use efficiency sustains greening at higher CWD levels (Zhu et al., 2016; Donohue et al., 2013; van der Sleen et al., 2015; Beer et al., 2010; Piao et al., 2019). The slower greening rates, or even browning in some regions, are consistent with water availability and atmospheric demand becoming stronger constraints at the high-deficit end of the drydown (Novick et al., 2016; Jiao et al., 2021; Zhou et al., 2019). Browning of the low state is found predominantly in humid regions, which at first might seem counterintuitive, as higher soil water availability could be expected to sustain higher values of CWD. However, these regions show the most pronounced declining trends in CWD. Therefore, it is possible that browning might reflect a limited ability of vegetation in those regions to adapt to the fast pace of changing hydrometeorological conditions. Because these drivers are inferred from the co-occurrence of greenness and cumulative-deficit trends rather than from formal attribution, they should be treated as candidate explanations rather than established causes.

The widening between the two states therefore suggests that greening processes may still dominate the favourable part of the drydown when CWD is moderate and other limiting factors are more relevant, while increasing water limitation becomes more visible later in the drydown. This split shows that the low state does not follow a single trajectory across climate zones. The contrast between a greening peak and a weaker or browning low state is consistent with an overshoot-like response, where greenness increases at the peak state but is not maintained once cumulative deficit becomes larger (Jump et al., 2017; Zhang et al., 2021). However, as we compare trends at two drydown states rather than tracking canopy development directly, we interpret this as consistent with such a mechanism, not as evidence for it.

https://doi.org/10.5194/egusphere-2026-5509
Preprint. Discussion started: 29 September 2026
© Author(s) 2026. CC BY 4.0 License.

Some regions show localised browning at both states (Fig. 4). Some of these patterns co-occurred with increasing CWD. In the energy-limited Cold Humid zone, for example, approximately 25 % of grid cells showed peak-state browning together with an increasing associated CWD, forming a secondary lobe in the browning–drying quadrant of the Fig. 5 distribution (Table A13). However, browning may also reflect broader ecological changes, particularly where both greenness states decline, as observed in parts of the energy-limited high latitudes (Fig. 4a). Drought and heat can leave legacy effects on growth and carbon uptake, and disturbance, deforestation or mortality can alter canopy greenness independently of the current drydown (Bastos et al., 2020a; Kannenberg et al., 2020; McDowell et al., 2023; Bourgoin et al., 2024), including in boreal and high-latitude forests affected by fire and drought (Webb et al., 2024; Fan et al., 2023). We therefore interpret these browning classes as possible imprints of water stress or disturbance legacies, rather than as direct evidence of physiological drought stress from CWD alone.

4.4 Shifts in hydrometeorological regime during extreme years

The predominance of greening trends appears to contradict studies reporting an increase in browning trends associated with water limitation (Denissen et al., 2022). This apparent mismatch can be explained by temporary shifts from energy limitation to water limitation driven by extreme drought, in regions predominantly associated with the energy-limited regime (Fig. 6). Our analysis of joint EVI–CWD dynamics allows us to capture shifts over western Russia in 2010 that coincided with the compound heatwave and drought (Flach et al., 2018). However, biosphere responses to that event were spatially heterogeneous and could not be unequivocally attributed to water limitation (Bastos et al., 2014; Flach et al., 2018). The same year, the Amazon experienced a severe drought and widespread browning (Xu et al., 2011; Lewis et al., 2011). In central Europe, shifts in 2015 overlapped with a summer during which regional precipitation was the lowest recorded since 1901 (Orth et al., 2016) while those in 2018 coincided with the heat and drought event that reduced ecosystem productivity across central and northern Europe (Bastos et al., 2020b). Generally, the higher occurrence of such shifts in temperate zones (Table A14) further suggests that the persistence of the hydrometeorological regime under increasing CWD differs among climate backgrounds, and that temperate regions are particularly sensitive to drought extremes (Fig. 6; Table A14).

Our results resolve a different temporal expression of water limitation from the longer-term shift reported by Denissen et al. (2022), who derived an ecosystem limitation index from Earth system model simulations over 1980–2100. They found increasing water limitation across about 73 % of the warm land area over 1980–2100, with the water-limited fraction expanding from 70 % to 77 %. The strongest trends occurred partly across Northern

Hemisphere mid-latitudes, broadly corresponding to the temperate regions where shifts were most frequent in our analysis (Table A14). However, we do not find significant trends in the areas affected by shifts from EL to WL across climate zones (Fig. A6). Whereas their analysis pointed to changes in the prevailing limitation regime over decadal timescales, our results show temporary water-limited behaviour within ecosystems that remain predominantly energy-limited over the observational period.

4.5 Limitations

We note that several factors not explicitly resolved here are also likely to influence the observed EVI–CWD trajectories. Changes in land use and management, vegetation composition, disturbance history and associated legacy effects may alter canopy greenness independently of the concurrent cumulative water deficit, and should be considered in future studies. In addition, repeated drydowns at the same location do not occur under stationary background conditions: both the physical environment and vegetation itself have changed through warming, shifting precipitation seasonality, rising atmospheric demand, CO_2 fertilisation, land-use change and disturbance legacies. EVI also measures canopy greenness rather than photosynthesis, biomass or plant water status, while CWD is an accumulated atmospheric–hydrological deficit rather than a direct measure of soil moisture or plant water availability. Furthermore, increasing canopy cover can also increase evapotranspiration (Zeng et al., 2018; Yang et al., 2023), possibly contributing to CWD trends. Our trend analysis therefore captures the co-evolution of greenness and cumulative deficit, but does not formally attribute these trajectories to individual drivers, nor does it quantify physiological drought stress. Drydown events capture vegetation resistance to an accumulating water deficit (Ingrisch and Bahn, 2018), but do not consider subsequent recovery (Schwalm et al., 2017), so our results concern resistance rather than recovery. Consequently, although some annual shifts coincided spatially with documented extreme events, these spatial overlaps do not identify which process caused the shift in any given pixel, since several drivers can reduce greenness in the same regions.

Across 2000–2023, the area expressing water-limited behaviour varied among years and showed no apparent directional change (Fig. A6). Our results therefore do not provide evidence for a progressive transition from energy to water limitation over the observational period, although the length of the record limits our ability to distinguish interannual variability from an emerging trend.

Finally, drydown timing and duration vary across climate zones, so the peak and low states do not always fall in the same seasonal window across regions. This is, however, more a strength than a limitation of the event-relative approach: because each response is measured against its own accumulating deficit, our framework does not impose a fixed calendar window and does not require prior de-seasonalisation of the EVI signal, unlike anomaly-

https://doi.org/10.5194/egusphere-2026-5509
Preprint. Discussion started: 29 September 2026
© Author(s) 2026. CC BY 4.0 License.

based or aggregated sensitivity metrics. The residual caveat is in cold regions, where snow accumulation and snowmelt affect both CWD and the satellite greenness signal, and where deficit accumulation can begin during spring green-up; we limit this by focusing on the annual-maximum drydown, which mostly falls between spring and late summer (Fig. A2). Nevertheless, analysing vegetation change along drydown trajectories reveals contrasts in the direction, steepness and long-term change of greenness responses that seasonal anomalies or aggregated sensitivity metrics would not capture.

5 Conclusions

Our study aimed to analyse how vegetation greenness responds dynamically to accumulating water deficits during drydowns. By resolving each drydown as a transition between peak and low greenness states, we show that ecosystems differ not only in whether greenness increases or decreases with cumulative water deficit, but also in how wide the deficit window is between these two states. Across climate zones, similar relative changes in greenness can occur over very different cumulative-deficit ranges, showing that comparable greenness responses can develop across contrasting hydrological conditions.

This within-event perspective also reveals contrasts that would be missed by seasonal anomalies or single sensitivity metrics. Energy-limited pixels, predominating across cold extratropical regions, often showed increasing greenness as water deficit accumulated, whereas water-limited pixels showed a peak followed by lower greenness at higher cumulative deficit, a configuration consistent with a non-linear rise-then-decline response. Over 2000–2023, the peak and low EVI states increased across nearly all climate-zone and regime combinations, including in water-limited regions, but the low state showed either slower greening than the peak or browning in some regions. In Cold Humid water-limited regions, the low-state mode combined browning with an increasing temporal trend in the associated CWD. This suggests that global greening signals can coexist with increasing water deficits, while the contrasting behaviour of the peak and low states is consistent with an overshoot-like response in some regions.

Our analysis of vegetation responses to drought as trajectories rather than isolated anomalies therefore provides a more complete perspective on how ecosystems withstand accumulating water deficit, with implications for anticipating changes in vegetation resistance, land–atmosphere feedbacks and terrestrial carbon–water cycling under continued warming.

https://doi.org/10.5194/egusphere-2026-5509
Preprint. Discussion started: 29 September 2026
© Author(s) 2026. CC BY 4.0 License.

Appendix A Supplementary analyses

A1 Drydown states

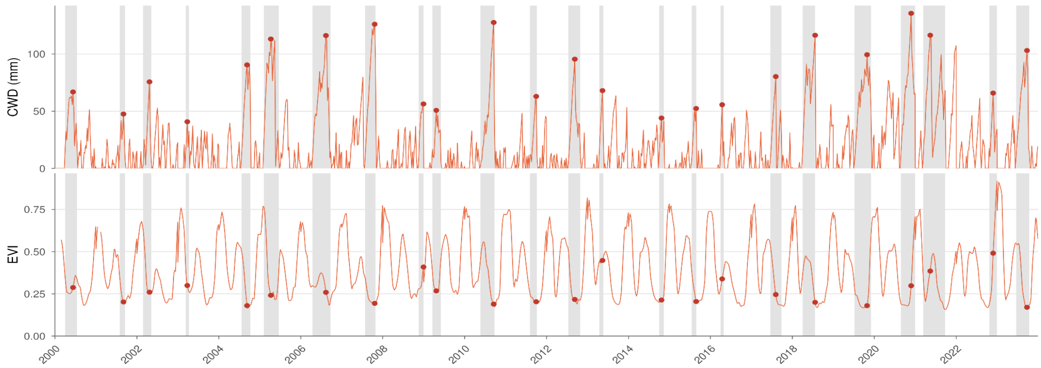

Figure A1: Example single-pixel weekly series (temperate-humid; 23.15°S, 51.35°W, 2000–2023) of cumulative water deficit (CWD, top) and EVI (bottom). Grey bands span each year's maximum drydown; red dots mark its peak CWD and co-occurring EVI.

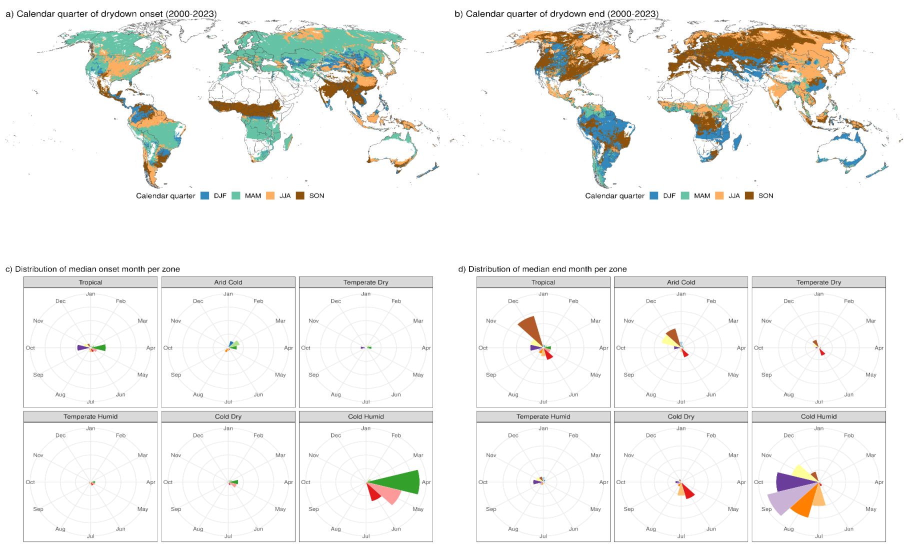

Figure A2: Timing of the annual-maximum drydowns across climate zones (2000–2023). For each grid cell, the annual-maximum drydown (Sect. 2.5) was identified in each year, and its onset and end months were summarised across years using the circular median. (a) Calendar quarter of drydown onset and (b) calendar quarter of drydown end (DJF = December–February, MAM = March–May, JJA = June–August, SON = September–November). (c, d) Distribution of the median onset and end month across grid cells, by climate zone. Maps and rose diagrams use the raw calendar month, without hemisphere adjustment, so a given quarter denotes the same months in both hemispheres. These panels describe the timing of the drydown event.

https://doi.org/10.5194/egusphere-2026-5509
Preprint. Discussion started: 29 September 2026
© Author(s) 2026. CC BY 4.0 License.

Table A1: Fraction of grid cells classified as energy-limited (EL) or water-limited (WL) in each climate zone. Percentages are area-weighted by grid-cell area (cos latitude); n = total grid cells per zone.

Climate zone	EL (%)	WL (%)	n
Tropical	32.9	67.1	229,411
Arid Cold	58.9	41.1	116,926
Temperate Dry	20.0	80.0	69,941
Temperate Humid	40.8	59.2	85,325
Cold Dry	86.5	13.5	106,142
Cold Humid	86.9	13.1	388,254

620 **Table A2: Distributions of the six Figure 2 variables by climate zone and drydown regime. Medians with the interquartile range [Q25, Q75]; Skew is the Bowley (quartile) coefficient. EL = energy-limited (greenness rises as the deficit accumulates); WL = water-limited (declines). Statistics are per grid cell. n = grid cells.**

Climate zone	Regime	n	Median [Q25, Q75]	Skewness
EVI_{95}				
Tropical	EL	74,625	0.596 [0.545, 0.628]	-0.24
Tropical	WL	154,786	0.511 [0.443, 0.575]	-0.04
Arid Cold	EL	69,068	0.225 [0.156, 0.301]	0.04
Arid Cold	WL	47,858	0.28 [0.21, 0.345]	-0.04
Temperate Dry	EL	14,610	0.475 [0.384, 0.552]	-0.08
Temperate Dry	WL	55,331	0.44 [0.382, 0.501]	0.02
Temperate Humid	EL	36,030	0.532 [0.47, 0.583]	-0.09
Temperate Humid	WL	49,295	0.544 [0.484, 0.602]	-0.02
Cold Dry	EL	94,587	0.417 [0.357, 0.491]	0.10
Cold Dry	WL	11,555	0.327 [0.245, 0.407]	-0.02
Cold Humid	EL	346,934	0.432 [0.368, 0.503]	0.04
Cold Humid	WL	41,320	0.495 [0.411, 0.572]	-0.05

https://doi.org/10.5194/egusphere-2026-5509
Preprint. Discussion started: 29 September 2026
© Author(s) 2026. CC BY 4.0 License.

Climate zone	Regime	n	Median [Q25, Q75]	Skewness
EVI_{05}				
Tropical	EL	74,625	0.419 [0.303, 0.454]	-0.53
Tropical	WL	154,786	0.224 [0.172, 0.33]	0.34
Arid Cold	EL	69,068	0.058 [0.018, 0.091]	-0.10
Arid Cold	WL	47,858	0.052 [0.015, 0.108]	0.20
Temperate Dry	EL	14,610	0.174 [0.135, 0.239]	0.25
Temperate Dry	WL	55,331	0.185 [0.148, 0.237]	0.18
Temperate Humid	EL	36,030	0.242 [0.193, 0.288]	-0.02
Temperate Humid	WL	49,295	0.246 [0.203, 0.291]	0.02
Cold Dry	EL	94,587	0.024 [0.011, 0.063]	0.49
Cold Dry	WL	11,555	0.038 [0.012, 0.105]	0.46
Cold Humid	EL	346,934	0.043 [0.019, 0.105]	0.43
Cold Humid	WL	41,320	0.073 [0.018, 0.136]	0.07
ΔEVI (%)				
Tropical	EL	74,625	30.5 [27.2, 43.7]	0.60
Tropical	WL	154,786	-52.2 [-62.3, -38.9]	0.14
Arid Cold	EL	69,068	71.4 [51.5, 92.2]	0.02
Arid Cold	WL	47,858	-77.2 [-94.2, -60.8]	-0.02
Temperate Dry	EL	14,610	56.7 [43, 70.4]	0.00
Temperate Dry	WL	55,331	-55.8 [-63.9, -46.6]	0.06
Temperate Humid	EL	36,030	53.3 [44.1, 62.3]	-0.02
Temperate Humid	WL	49,295	-53.7 [-62, -44.8]	0.04
Cold Dry	EL	94,587	94 [85.4, 97.1]	-0.47

Climate zone	Regime	n	Median [Q25, Q75]	Skewness
Cold Dry	WL	11,555	-87.7 [-95.4, -67.1]	0.46
Cold Humid	EL	346,934	89.4 [77.9, 95]	-0.34
Cold Humid	WL	41,320	-84.7 [-96, -73.2]	0.01
CWD_{EVI95} (mm)				
Tropical	EL	74,625	126.6 [60.8, 206.4]	0.10
Tropical	WL	154,786	39.9 [23.7, 75.9]	0.38
Arid Cold	EL	69,068	34.8 [19.9, 58.3]	0.23
Arid Cold	WL	47,858	29.3 [18.2, 51.4]	0.33
Temperate Dry	EL	14,610	44.3 [22.4, 81.4]	0.26
Temperate Dry	WL	55,331	27 [19.2, 44.5]	0.38
Temperate Humid	EL	36,030	42.1 [29.3, 58.8]	0.13
Temperate Humid	WL	49,295	31.8 [23.4, 42.6]	0.12
Cold Dry	EL	94,587	40.7 [23.1, 64]	0.14
Cold Dry	WL	11,555	24.2 [13.3, 41.5]	0.23
Cold Humid	EL	346,934	55.2 [35.9, 79.3]	0.11
Cold Humid	WL	41,320	32.8 [18.1, 52.3]	0.14
CWD_{EVI05} (mm)				
Tropical	EL	74,625	59.1 [31.3, 94.6]	0.12
Tropical	WL	154,786	151.5 [81, 221.3]	-0.01
Arid Cold	EL	69,068	11.5 [6.1, 23.8]	0.40
Arid Cold	WL	47,858	64.1 [35.5, 91.2]	-0.03
Temperate Dry	EL	14,610	17.2 [9.1, 38.4]	0.45
Temperate Dry	WL	55,331	124.6 [71.6, 190.1]	0.10

https://doi.org/10.5194/egusphere-2026-5509
Preprint. Discussion started: 29 September 2026
© Author(s) 2026. CC BY 4.0 License.

Climate zone	Regime	n	Median [Q25, Q75]	Skewness
Temperate Humid	EL	36,030	20 [12.7, 31.5]	0.23
Temperate Humid	WL	49,295	70.3 [47.6, 99.4]	0.12
Cold Dry	EL	94,587	6.2 [3.7, 10.8]	0.30
Cold Dry	WL	11,555	68.7 [21.1, 114.8]	-0.02
Cold Humid	EL	346,934	10.2 [6.9, 17.1]	0.35
Cold Humid	WL	41,320	55.4 [31.1, 81.2]	0.03
ΔCWD (mm)				
Tropical	EL	74,625	44.7 [13.2, 107.8]	0.33
Tropical	WL	154,786	80.8 [31.5, 150.3]	0.17
Arid Cold	EL	69,068	15.7 [7.8, 30.8]	0.31
Arid Cold	WL	47,858	21.9 [8.5, 45.7]	0.28
Temperate Dry	EL	14,610	18.3 [7.9, 41.5]	0.38
Temperate Dry	WL	55,331	82.5 [39.6, 134.1]	0.09
Temperate Humid	EL	36,030	16.8 [7.6, 31.2]	0.22
Temperate Humid	WL	49,295	32.8 [13.5, 60.9]	0.19
Cold Dry	EL	94,587	32.1 [16.1, 51.2]	0.09
Cold Dry	WL	11,555	27.7 [5.3, 69.5]	0.30
Cold Humid	EL	346,934	38.9 [21.6, 60.9]	0.12
Cold Humid	WL	41,320	13.8 [4.7, 29.8]	0.28

https://doi.org/10.5194/egusphere-2026-5509
Preprint. Discussion started: 29 September 2026
© Author(s) 2026. CC BY 4.0 License.

625 **Table A3: Zone effect on ΔEVI and ΔCWD within each regime. H = Kruskal–Wallis statistic across the six zones (df = 5); ε² = epsilon-squared effect size. All tests have p < 0.001 given the sample sizes; differences interpreted by effect size. Per grid cell.**

Variable	Regime	n	Kruskal–Wallis H	ε²
ΔEVI	EL	635,854	283,316	0.446
ΔEVI	WL	360,145	127,501	0.354
ΔCWD	EL	635,854	60,479	0.095
ΔCWD	WL	360,145	85,469	0.237

Table A4: Pairwise Cliff's δ between climate zones for ΔEVI and ΔCWD in each regime. Each cell is δ (row vs column); positive means the row zone tends to exceed the column zone. Per grid cell.

ΔEVI: water-limited

	Trop	AriC	TempD	TempH	ColdD	ColdH
Trop	—					
AriC	-0.65	—				
TempD	-0.16	0.59	—			
TempH	-0.08	0.62	0.09	—		
ColdD	-0.78	-0.16	-0.73	-0.76	—	
ColdH	-0.88	-0.24	-0.86	-0.87	-0.06	—

630 **ΔEVI: energy-limited**

	Trop	AriC	TempD	TempH	ColdD	ColdH
Trop	—					
AriC	0.76	—				
TempD	0.61	-0.38	—			
TempH	0.54	-0.45	-0.13	—		
ColdD	0.97	0.56	0.91	0.94	—	

https://doi.org/10.5194/egusphere-2026-5509
Preprint. Discussion started: 29 September 2026
© Author(s) 2026. CC BY 4.0 License.

	Trop	AriC	TempD	TempH	ColdD	ColdH
ColdH	0.95	0.40	0.84	0.92	-0.26	—

ΔCWD: water-limited

	Trop	AriC	TempD	TempH	ColdD	ColdH
Trop	—					
AriC	-0.54	—				
TempD	-0.01	0.59	—			
TempH	-0.43	0.17	-0.48	—		
ColdD	-0.47	0.06	-0.50	-0.08	—	
ColdH	-0.68	-0.22	-0.73	-0.39	-0.23	—

ΔCWD: energy-limited

	Trop	AriC	TempD	TempH	ColdD	ColdH
Trop	—					
AriC	-0.40	—				
TempD	-0.34	0.08	—			
TempH	-0.41	0.00	-0.08	—		
ColdD	-0.18	0.36	0.24	0.36	—	
ColdH	-0.09	0.48	0.36	0.48	0.15	—

635 *Zones: Trop Tropical, AriC Arid Cold, TempD Temperate Dry, TempH Temperate Humid, ColdD Cold Dry, ColdH Cold Humid. Greyscale shading indicates effect-size magnitude: white < 0.15 negligible, light grey 0.15–0.33 small, medium grey 0.33–0.47 medium, dark grey ≥ 0.47 large.*

https://doi.org/10.5194/egusphere-2026-5509
Preprint. Discussion started: 29 September 2026
© Author(s) 2026. CC BY 4.0 License.

Table A5: Within-zone contrast between the energy-limited (EL) and water-limited (WL) regimes. Median of EL cells, median of WL cells, and Cliff's δ comparing them (δ > 0 means EL > WL). ΔEVI omitted (sign fixed by regime). Per grid cell.

Climate zone	Median EL	Median WL	Cliff's δ (EL vs WL)
EVI_{95} (–)			
Tropical	0.596	0.511	0.48
Arid Cold	0.225	0.28	-0.26
Temperate Dry	0.475	0.44	0.14
Temperate Humid	0.532	0.544	-0.10
Cold Dry	0.417	0.327	0.47
Cold Humid	0.432	0.495	-0.27
EVI_{05} (–)			
Tropical	0.419	0.224	0.49
Arid Cold	0.058	0.052	-0.02
Temperate Dry	0.174	0.185	-0.07
Temperate Humid	0.242	0.246	-0.04
Cold Dry	0.024	0.038	-0.15
Cold Humid	0.043	0.073	-0.10
CWD_{EVI95} (mm)			
Tropical	126.6	39.9	0.53
Arid Cold	34.8	29.3	0.11
Temperate Dry	44.3	27	0.24
Temperate Humid	42.1	31.8	0.31
Cold Dry	40.7	24.2	0.34
Cold Humid	55.2	32.8	0.42

https://doi.org/10.5194/egusphere-2026-5509
Preprint. Discussion started: 29 September 2026
© Author(s) 2026. CC BY 4.0 License.

Climate zone	Median EL	Median WL	Cliff's δ (EL vs WL)
CWD_{EVI05} (mm)			
Tropical	59.1	151.5	-0.57
Arid Cold	11.5	64.1	-0.78
Temperate Dry	17.2	124.6	-0.83
Temperate Humid	20	70.3	-0.81
Cold Dry	6.2	68.7	-0.81
Cold Humid	10.2	55.4	-0.73
ΔCWD (mm)			
Tropical	44.7	80.8	-0.23
Arid Cold	15.7	21.9	-0.14
Temperate Dry	18.3	82.5	-0.63
Temperate Humid	16.8	32.8	-0.33
Cold Dry	32.1	27.7	0.06
Cold Humid	38.9	13.8	0.53

https://doi.org/10.5194/egusphere-2026-5509
Preprint. Discussion started: 29 September 2026
© Author(s) 2026. CC BY 4.0 License.

A2 Vegetation sensitivity to drought

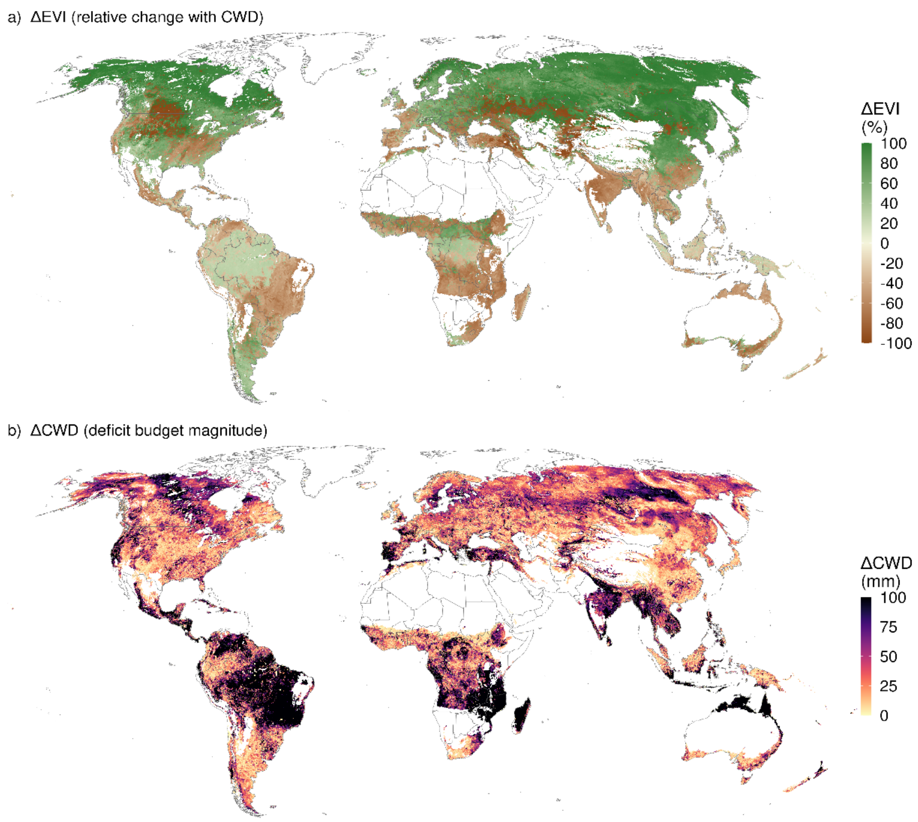

Figure A3: Relative greenness change (ΔEVI) and deficit budget (ΔCWD) between the peak and low greenness states. Global maps per grid cell from the pooled peak and low states across annual maximum drydowns, 2000–2023. (a) ΔEVI (%); (b) ΔCWD (mm). Per-zone values in Table A2.

Table A6: Distribution of the EVI–CWD sensitivity S (= ΔEVI/ΔCWD, % mm^{-1}) by climate zone and drydown regime. Values are medians with the interquartile range [Q25, Q75]; P05 and P95 are the 5th and 95th percentiles; Skew is the Bowley (quartile) coefficient. WL = water-limited (S < 0), EL = energy-limited (S > 0). n = grid cells with ΔCWD > 5 mm.

Climate zone	n	Median [Q25, Q75]	P05	P95	Skew
Water-limited (WL)					
Cold Humid	30,492	-3.93 [-7.21, -2.26]	-14.07	-1.12	-0.33
Arid Cold	40,079	-2.72 [-5.29, -1.4]	-11.88	-0.54	-0.32

https://doi.org/10.5194/egusphere-2026-5509
Preprint. Discussion started: 29 September 2026
© Author(s) 2026. CC BY 4.0 License.

Climate zone	n	Median [Q25, Q75]	P05	P95	Skew
Cold Dry	8,743	-1.71 [-4.44, -0.97]	-12.73	-0.51	-0.57
Temperate Humid	43,828	-1.41 [-2.76, -0.78]	-6.98	-0.37	-0.36
Temperate Dry	52,942	-0.64 [-1.23, -0.39]	-4.27	-0.24	-0.41
Tropical	146,192	-0.57 [-1.26, -0.32]	-4.51	-0.18	-0.47
Energy-limited (EL)					
Tropical	65,928	0.63 [0.27, 1.63]	0.12	6.73	0.48
Cold Humid	333,034	2.1 [1.37, 3.59]	0.84	8.76	0.34
Temperate Dry	12,213	2.33 [1.04, 4.95]	0.4	10	0.34
Temperate Humid	29,722	2.48 [1.48, 4.29]	0.65	8.46	0.29
Cold Dry	89,201	2.65 [1.71, 4.78]	1.01	11.14	0.39
Arid Cold	58,499	3.46 [1.84, 6.34]	0.78	12.23	0.28

Table A7: Zone effect on S within each regime. H = Kruskal–Wallis statistic across the six zones (df = 5); ε^2 = epsilon-squared effect size. Both $p < 0.001$ given the sample sizes; differences are interpreted by effect size.

Regime	n	Kruskal–Wallis H	ε^2
Water-limited (WL)	322,276	101,177	0.314
Energy-limited (EL)	588,597	79,574	0.135

https://doi.org/10.5194/egusphere-2026-5509
Preprint. Discussion started: 29 September 2026
© Author(s) 2026. CC BY 4.0 License.

Table A8: Pairwise Cliff's δ between climate zones for S: water-limited regime. Each cell is δ (row vs column); positive means the row zone has the less negative (shallower) S.

	Trop	AriC	TempD	TempH	ColdD	ColdH
Trop	—					
AriC	-0.68	—				
TempD	-0.08	0.67	—			
TempH	-0.46	0.35	-0.44	—		
ColdD	-0.58	0.17	-0.57	-0.17	—	
ColdH	-0.82	-0.24	-0.82	-0.59	-0.40	—

Zones: Trop Tropical, AriC Arid Cold, TempD Temperate Dry, TempH Temperate Humid, ColdD Cold Dry, ColdH Cold Humid. Greyscale shading indicates effect-size magnitude: white < 0.15 negligible, light grey 0.15–0.33 small, medium grey 0.33–0.47 medium, dark grey ≥ 0.47 large.

Table A9: Pairwise Cliff's δ between climate zones for S: energy-limited regime. Each cell is δ (row vs column); positive means the row zone has the larger (steeper) positive S. Greyscale shading as in Table A8.

	Trop	AriC	TempD	TempH	ColdD	ColdH
Trop	—					
AriC	0.68	—				
TempD	0.52	-0.23	—			
TempH	0.60	-0.21	0.05	—		
ColdD	0.66	-0.12	0.14	0.10	—	
ColdH	0.59	-0.28	0.00	-0.09	-0.19	—

https://doi.org/10.5194/egusphere-2026-5509
Preprint. Discussion started: 29 September 2026
© Author(s) 2026. CC BY 4.0 License.

A3 Direction of EVI trends at the peak and low states

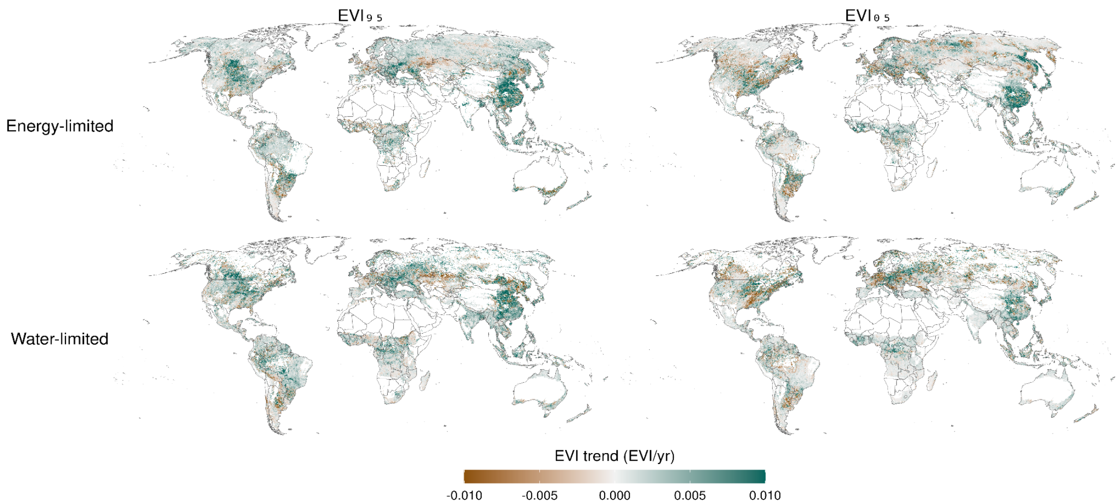

Figure A4: Per-pixel EVI trends (Theil–Sen slope, EVI yr^{-1}) for the high (EVI_{95}) and low (EVI_{05}) drydown states, split by energy- vs water-limited regime. Brown = decline, teal = greening; scale clipped at ±0.01.

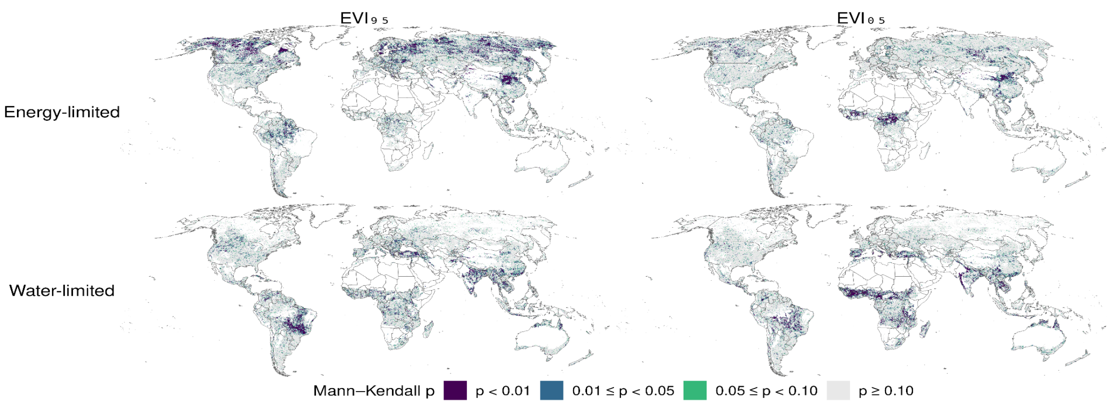

Figure A5: Statistical significance of the EVI trends. Per-grid-cell Mann–Kendall p-values for the Theil–Sen trends underlying Figs. 4 and 5, shown for the peak (EVI_{95}) and low (EVI_{05}) greenness states (columns) in the energy-limited and water-limited regimes (rows). Colours bin the p-value into $p < 0.01$, $0.01 \leq p < 0.05$, $0.05 \leq p < 0.10$ and $p \geq 0.10$ (non-significant, light grey).

https://doi.org/10.5194/egusphere-2026-5509
Preprint. Discussion started: 29 September 2026
© Author(s) 2026. CC BY 4.0 License.

Table A10: Area-weighted distribution of grid cells across the four EVI trend-direction classes, by regime. Percentages are weighted by grid-cell area (cos latitude) and are given for all classified grid cells and for the subset with a significant trend (Mann–Kendall $p < 0.05$) in at least one greenness state; n is the number of grid cells. Peak = EVI_{95}, low = EVI_{05}.

EVI trend class	Energy-limited (all)	Energy-limited (significant)	Water-limited (all)	Water-limited (significant)
EVI_{95} ↑ / EVI_{05} ↑	46.8 %	61.7 %	48.1 %	64.9 %
EVI_{95} ↑ / EVI_{05} ↓	24.1 %	21.3 %	20.6 %	14.2 %
EVI_{95} ↓ / EVI_{05} ↑	15.2 %	9.1 %	16.8 %	12.1 %
EVI_{95} ↓ / EVI_{05} ↓	14.0 %	7.9 %	14.5 %	8.7 %
n (grid cells)	*798,961*	*233,635*	*632,280*	*154,975*

Arrows: ↑ increasing trend, ↓ decreasing trend (Theil–Sen slope, 2000–2023).

Table A11: Area-weighted distribution of grid cells across the four EVI trend-direction classes, by climate zone and regime. Percentages are weighted by grid-cell area (cos latitude) and sum to 100 % within each zone. Peak = EVI_{95}, low = EVI_{05}; arrows denote increasing (↑) or decreasing (↓) Theil–Sen trends over 2000–2023.

Energy-limited

Climate zone	EVI_{95} ↑ / EVI_{05} ↑	EVI_{95} ↓ / EVI_{05} ↑	EVI_{95} ↓ / EVI_{05} ↓	EVI_{95} ↑ / EVI_{05} ↓
Arid Cold	41.4 %	21.1 %	19.1 %	18.4 %
Cold Dry	51.7 %	11.6 %	11.3 %	25.4 %
Cold Humid	44.4 %	11.5 %	14 %	30.2 %
Temperate Dry	57.3 %	18.3 %	11.4 %	13 %
Temperate Humid	42.3 %	18 %	18.9 %	20.8 %
Tropical	52 %	17.2 %	10 %	20.8 %

Water-limited

Climate zone	EVI_{95} ↑ / EVI_{05} ↑	EVI_{95} ↓ / EVI_{05} ↑	EVI_{95} ↓ / EVI_{05} ↓	EVI_{95} ↑ / EVI_{05} ↓
Arid Cold	43.2 %	21.1 %	18.9 %	16.8 %
Cold Dry	46.8 %	18 %	16.5 %	18.6 %
Cold Humid	39 %	13.7 %	15.9 %	31.4 %
Temperate Dry	59.6 %	16.6 %	10.7 %	13.1 %
Temperate Humid	41 %	15.7 %	20.5 %	22.7 %
Tropical	52.9 %	16.7 %	11.2 %	19.2 %

685 **Table A12: Two-dimensional mode (peak of the kernel density) of each state's bivariate distribution of per-decade Sen slopes. n = number of grid cells with a significant EVI or CWD trend used in the bivariate KDE. States: peak, low. Regimes: energy-limited (EL), water-limited (WL). CWD mode in mm decade^{-1} (>0 = drying), EVI mode in decade^{-1} (>0 = greening). See Sect. 2.9.**

Climate zone	State	n	CWD mode	EVI mode
Energy-limited (EL)				
Tropical	peak	2,103	67.6	0.025
Tropical	low	2,523	33.6	0.022
Arid Cold	peak	1,314	−19.8	0.019
Arid Cold	low	711	8.0	0.018
Temperate Dry	peak	308	−46.5	0.095
Temperate Dry	low	304	8.9	0.055
Temperate Humid	peak	437	−52.9	0.035
Temperate Humid	low	243	11.1	0.068
Cold Dry	peak	1,699	22.1	0.022
Cold Dry	low	954	3.6	0.033

https://doi.org/10.5194/egusphere-2026-5509
Preprint. Discussion started: 29 September 2026
© Author(s) 2026. CC BY 4.0 License.

Climate zone	State	n	CWD mode	EVI mode
Cold Humid	peak	6,593	28.0	0.020
Cold Humid	low	2,730	6.5	0.020
Water-limited (WL)				
Tropical	peak	4,277	8.9	0.028
Tropical	low	7,061	−13.4	0.009
Arid Cold	peak	766	−15.9	0.011
Arid Cold	low	971	−26.7	0.007
Temperate Dry	peak	1,044	7.5	0.036
Temperate Dry	low	2,335	−23.7	0.007
Temperate Humid	peak	363	18.3	0.047
Temperate Humid	low	520	−46.1	0.032
Cold Dry	peak	265	−18.4	0.026
Cold Dry	low	269	33.1	0.010
Cold Humid	peak	640	40.5	0.069
Cold Humid	low	415	87.4	−0.069

690 **Table A13: Fraction of grid cells (%) in each trajectory per state, regime and climate zone: GD greening–drying, GA greening–attenuating, BD browning–drying, BA browning–attenuating (rows sum to 100).**

Climate zone	State	GD	GA	BD	BA
Energy-limited (EL)					
Tropical	peak	74.6	15.7	3.8	5.8
Tropical	low	77.4	14.5	5.1	3.1
Arid Cold	peak	20.3	44.2	8.2	27.2

https://doi.org/10.5194/egusphere-2026-5509
Preprint. Discussion started: 29 September 2026
© Author(s) 2026. CC BY 4.0 License.

Climate zone	State	GD	GA	BD	BA
Arid Cold	low	43.5	28.1	5.1	23.3
Temperate Dry	peak	38.6	47.1	3.2	11.0
Temperate Dry	low	55.3	22.7	2.6	19.4
Temperate Humid	peak	30.7	46.7	9.6	13.0
Temperate Humid	low	43.2	30.0	14.4	12.3
Cold Dry	peak	54.9	33.1	4.1	7.9
Cold Dry	low	60.4	17.0	3.2	19.4
Cold Humid	peak	60.3	13.6	24.8	1.3
Cold Humid	low	50.7	17.6	13.1	18.7
Water-limited (WL)					
Tropical	peak	68.8	14.5	4.7	12.0
Tropical	low	35.9	40.9	3.7	19.5
Arid Cold	peak	35.8	36.9	10.3	17.0
Arid Cold	low	29.1	48.2	1.8	20.9
Temperate Dry	peak	59.1	24.9	5.5	10.5
Temperate Dry	low	46.4	35.2	2.3	16.1
Temperate Humid	peak	46.8	24.5	13.2	15.4
Temperate Humid	low	16.0	40.8	37.3	6.0
Cold Dry	peak	38.9	47.9	4.9	8.3
Cold Dry	low	70.6	16.7	7.8	4.8
Cold Humid	peak	69.4	18.0	8.9	3.8
Cold Humid	low	31.1	18.6	42.9	7.5

https://doi.org/10.5194/egusphere-2026-5509
Preprint. Discussion started: 29 September 2026
© Author(s) 2026. CC BY 4.0 License.

Table A14: EL→WL shift rate by climate zone (%).

Climate zone	2010	2015	2018
Tropical	33.9	26.1	30.3
Arid Cold	29.8	36.7	39.5
Temperate Dry	48.2	37.3	46.7
Temperate Humid	42.5	39.7	46.4
Cold Dry	13.9	12.9	19.0
Cold Humid	13.7	19.1	12.4
Global (all zones)	**22.5**	**23.5**	**22.5**

EL→WL shift rate: area-weighted percentage of climatologically energy-limited (EL) grid cells that shifted to water-limited (WL) behaviour in each year (i.e., $CWD_{EVI05} > CWD_{EVI95}$*). The global row is area-weighted across all zones.*

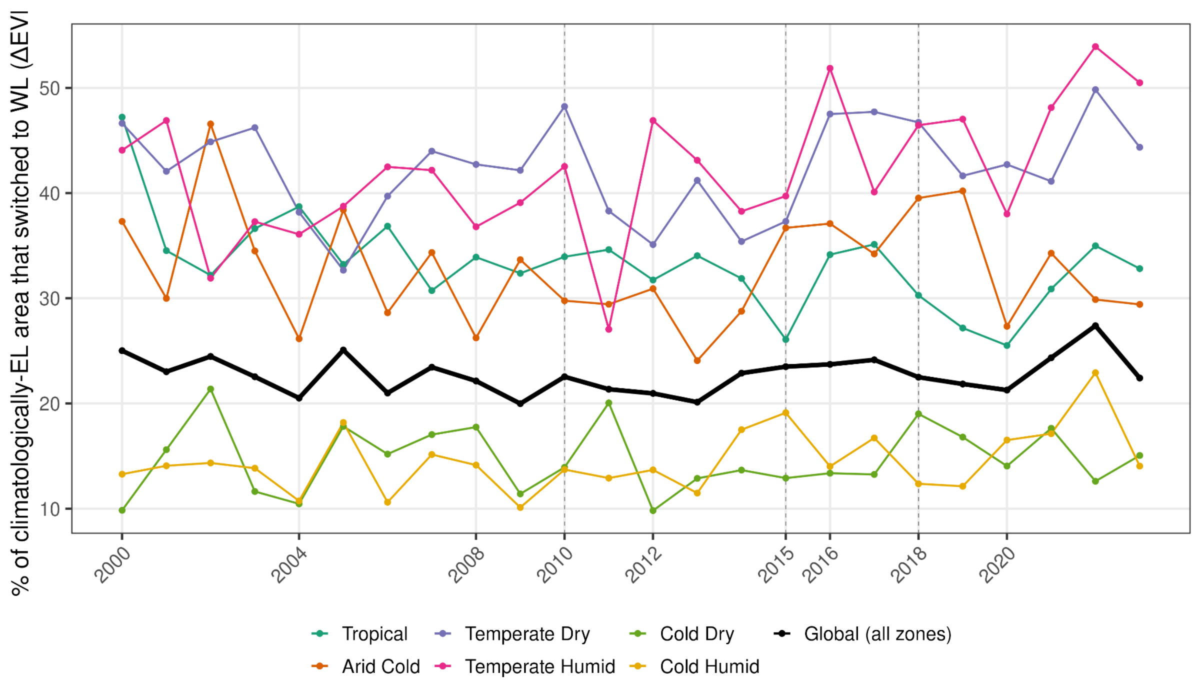

Figure A6: Annual fraction of energy-limited area shifting to water-limited behaviour, 2000–2023.

https://doi.org/10.5194/egusphere-2026-5509
Preprint. Discussion started: 29 September 2026
© Author(s) 2026. CC BY 4.0 License.

Code and data availability

All input data supporting the findings of this study are freely available from public sources: MODIS MOD13C1 v6.1 EVI data from the NASA LP DAAC (https://doi.org/10.5067/MODIS/MOD13C1.061); MSWEP v2.8 precipitation data from GloH2O (https://www.gloh2o.org/mswep/); GLEAM v4.2a evapotranspiration data from https://www.gleam.eu; the Köppen–Geiger climate classification v2 (https://doi.org/10.6084/m9.figshare.21789074); ESA-CCI/C3S land-cover maps from the Copernicus Climate Data Store (https://doi.org/10.24381/cds.006f2c9a); and the GLDAS land-sea mask (https://ldas.gsfc.nasa.gov/gldas). The R code used to compute the cumulative water deficit, detect drydowns, derive the EVI–CWD states, sensitivities, regimes and trends, and produce all figures and tables is archived on Zenodo (https://doi.org/10.5281/zenodo.22917102) and is available at https://github.com/Mtrsh/drydowns-evi-cwd.

Author contribution

MT and AB designed the study. MT developed the analysis code, processed the datasets, performed the analysis and produced the figures. AB supervised the work and acquired the funding. SS and BDS contributed to the methodology and to the interpretation of the results. MT wrote the original draft, and all authors reviewed and edited the manuscript.

Competing interests

The authors declare that they have no conflict of interest.

Disclaimer

Publisher's note: "Copernicus Publications remains neutral with regard to jurisdictional claims made in the text, published maps, institutional affiliations, or any other geographical representation in this paper. While Copernicus Publications makes every effort to include appropriate place names, the final responsibility lies with the authors. Views expressed in the text are those of the authors and do not necessarily reflect the views of the publisher."

https://doi.org/10.5194/egusphere-2026-5509
Preprint. Discussion started: 29 September 2026
© Author(s) 2026. CC BY 4.0 License.

Acknowledgements

We thank Ulrich Weber (MPI-BGC) for technical support in preprocessing the datasets. Grammarly was used to check and improve the grammar and readability of some paragraphs of the manuscript.

Financial support

Ana Bastos acknowledges funding by the European Union (ERC StG, ForExD, grant agreement No. 101039567). This study received additional support from the European Space Agency Climate Change Initiative (ESA-CCI) Tipping Elements SIRENE project (contract no. 4000146954/24/I-LR) (MT).

https://doi.org/10.5194/egusphere-2026-5509
Preprint. Discussion started: 29 September 2026
© Author(s) 2026. CC BY 4.0 License.

References

Ahmad, S., McElwain, J., Nair, R., and Gill, L.: Comment on 'On the Use of the Term "Evapotranspiration"' by Miralles et al. (2020), Water Resour. Res., 61, e2024WR038835, https://doi.org/10.1029/2024WR038835, 2025.

Akbar, R., Short Gianotti, D. J., McColl, K. A., Haghighi, E., Salvucci, G. D., and Entekhabi, D.: Estimation of Landscape Soil Water Losses from Satellite Observations of Soil Moisture, J. Hydrometeorol., 19, 871–889, https://doi.org/10.1175/JHM-D-17-0200.1, 2018.

Anderegg, W. R. L., Trugman, A. T., Badgley, G., Konings, A. G., and Shaw, J.: Divergent forest sensitivity to repeated extreme droughts, Nat. Clim. Change, 10, 1091–1095, https://doi.org/10.1038/s41558-020-00919-1, 2020.

Bastos, A., Gouveia, C. M., Trigo, R. M., and Running, S. W.: Analysing the Spatio-Temporal Impacts of the 2003 and 2010 Extreme Heatwaves on Plant Productivity in Europe, Biogeosciences, 11, 3421–3435, https://doi.org/10.5194/bg-11-3421-2014, 2014.

Bastos, A., Ciais, P., Friedlingstein, P., Sitch, S., Pongratz, J., Fan, L., Wigneron, J. P., Weber, U., Reichstein, M., Fu, Z., Anthoni, P., Arneth, A., Haverd, V., Jain, A. K., Joetzjer, E., Knauer, J., Lienert, S., Loughran, T., McGuire, P. C., Tian, H., Viovy, N., and Zaehle, S.: Direct and Seasonal Legacy Effects of the 2018 Heat Wave and Drought on European Ecosystem Productivity, Sci. Adv., 6, eaba2724, https://doi.org/10.1126/sciadv.aba2724, 2020a.

Bastos, A., Fu, Z., Ciais, P., Friedlingstein, P., Sitch, S., Pongratz, J., Weber, U., Reichstein, M., Anthoni, P., Arneth, A., Haverd, V., Jain, A., Joetzjer, E., Knauer, J., Lienert, S., Loughran, T., McGuire, P. C., Obermeier, W., Padrón, R. S., Shi, H., Tian, H., Viovy, N., and Zaehle, S.: Impacts of extreme summers on European ecosystems: a comparative analysis of 2003, 2010 and 2018, Philos. Trans. R. Soc. B, 375, 20190507, https://doi.org/10.1098/rstb.2019.0507, 2020b.

Bastos, A., Orth, R., Reichstein, M., Ciais, P., Viovy, N., Zaehle, S., Anthoni, P., Arneth, A., Gentine, P., Joetzjer, E., Lienert, S., Loughran, T., McGuire, P. C., O, S., Pongratz, J., and Sitch, S.: Vulnerability of European ecosystems to two compound dry and hot summers in 2018 and 2019, Earth Syst. Dynam., 12, 1015–1035, https://doi.org/10.5194/esd-12-1015-2021, 2021.

Bastos, A., Sippel, S., Frank, D., Mahecha, M. D., Zaehle, S., Zscheischler, J., and Reichstein, M.: A joint framework for studying compound ecoclimatic events, Nat. Rev. Earth Environ., 4, 333–350, https://doi.org/10.1038/s43017-023-00410-3, 2023.

Beck, H. E., Vergopolan, N., Pan, M., Levizzani, V., van Dijk, A. I. J. M., Weedon, G. P., Brocca, L., Pappenberger, F., Huffman, G. J., and Wood, E. F.: Global-scale evaluation of 22 precipitation datasets using gauge observations and hydrological modeling, Hydrol. Earth Syst. Sci., 21, 6201–6217, https://doi.org/10.5194/hess-21-6201-2017, 2017.

Beck, H. E., Wood, E. F., Pan, M., Fisher, C. K., Miralles, D. G., van Dijk, A. I. J. M., McVicar, T. R., and Adler, R. F.: MSWEP V2 Global 3-Hourly 0.1° Precipitation: Methodology and Quantitative Assessment, Bull. Amer. Meteorol. Soc., 100, 473–500, https://doi.org/10.1175/BAMS-D-17-0138.1, 2019.

Beck, H. E., McVicar, T. R., Vergopolan, N., Berg, A., Lutsko, N. J., Dufour, A., Zeng, Z., Jiang, X., van Dijk, A. I. J. M., and Miralles, D. G.: High-resolution (1 km) Köppen-Geiger maps for 1901–2099 based on constrained CMIP6 projections, Sci. Data, 10, 724, https://doi.org/10.1038/s41597-023-02549-6, 2023.

Beer, C., Reichstein, M., Tomelleri, E., Ciais, P., Jung, M., Carvalhais, N., Rödenbeck, C., Arain, M. A., Baldocchi, D., Bonan, G. B., Bondeau, A., Cescatti, A., Lasslop, G., Lindroth, A., Lomas, M., Luyssaert, S.,

https://doi.org/10.5194/egusphere-2026-5509
Preprint. Discussion started: 29 September 2026
© Author(s) 2026. CC BY 4.0 License.

Margolis, H., Oleson, K. W., Roupsard, O., Veenendaal, E., Viovy, N., Williams, C., Woodward, F. I., and Papale, D.: Terrestrial Gross Carbon Dioxide Uptake: Global Distribution and Covariation with Climate, Science, 329, 834–838, https://doi.org/10.1126/science.1184984, 2010.

Bourgoin, C., Ceccherini, G., Girardello, M., Vancutsem, C., Avitabile, V., Beck, P. S. A., Beuchle, R., Blanc, L., Duveiller, G., Migliavacca, M., Vieilledent, G., Cescatti, A., and Achard, F.: Human Degradation of Tropical Moist Forests Is Greater than Previously Estimated, Nature, 631, 570–576, https://doi.org/10.1038/s41586-024-07629-0, 2024.

Brodribb, T. J., Powers, J., Cochard, H., and Choat, B.: Hanging by a thread? Forests and drought, Science, 368, 261–266, https://doi.org/10.1126/science.aat7631, 2020.

Buermann, W., Forkel, M., O'Sullivan, M., Sitch, S., Friedlingstein, P., Haverd, V., Jain, A. K., Kato, E., Kautz, M., Lienert, S., Lombardozzi, D., Nabel, J. E. M. S., Tian, H., Wiltshire, A. J., Zhu, D., Smith, W. K., and Richardson, A. D.: Widespread Seasonal Compensation Effects of Spring Warming on Northern Plant Productivity, Nature, 562, 110–114, https://doi.org/10.1038/s41586-018-0555-7, 2018.

Cao, R., Feng, Y., Liu, X., Shen, M., and Zhou, J.: Uncertainty of Vegetation Green-Up Date Estimated from Vegetation Indices Due to Snowmelt at Northern Middle and High Latitudes, Remote Sens., 12, 190, https://doi.org/10.3390/rs12010190, 2020.

Chitra-Tarak, R., Xu, C., Aguilar, S., Anderson-Teixeira, K. J., Chambers, J., Detto, M., Faybishenko, B., Fisher, R. A., Knox, R. G., Koven, C. D., Kueppers, L. M., Kunert, N., Kupers, S. J., McDowell, N. G., Newman, B. D., Paton, S. R., Pérez, R., Ruiz, L., Sack, L., Warren, J. M., Wolfe, B. T., Wright, C., Wright, S. J., Zailaa, J., and McMahon, S. M.: Hydraulically-vulnerable trees survive on deep-water access during droughts in a tropical forest, New Phytol., 231, 1798–1813, https://doi.org/10.1111/nph.17464, 2021.

Christina, M., Nouvellon, Y., Laclau, J.-P., Stape, J. L., Bouillet, J.-P., Lambais, G. R., and le Maire, G.: Importance of deep water uptake in tropical eucalypt forest, Funct. Ecol., 31, 509–519, https://doi.org/10.1111/1365-2435.12727, 2017.

Ciais, Ph., Reichstein, M., Viovy, N., Granier, A., Ogée, J., Allard, V., Aubinet, M., Buchmann, N., Bernhofer, Chr., Carrara, A., Chevallier, F., De Noblet, N., Friend, A. D., Friedlingstein, P., Grünwald, T., Heinesch, B., Keronen, P., Knohl, A., Krinner, G., Loustau, D., Manca, G., Matteucci, G., Miglietta, F., Ourcival, J. M., Papale, D., Pilegaard, K., Rambal, S., Seufert, G., Soussana, J. F., Sanz, M. J., Schulze, E. D., Vesala, T., and Valentini, R.: Europe-wide reduction in primary productivity caused by the heat and drought in 2003, Nature, 437, 529–533, https://doi.org/10.1038/nature03972, 2005.

Cliff, N.: Dominance statistics: ordinal analyses to answer ordinal questions, Psychol. Bull., 114, 494–509, https://doi.org/10.1037/0033-2909.114.3.494, 1993.

Copernicus Climate Change Service, Climate Data Store: Land Cover Classification Gridded Maps from 1992 to Present Derived from Satellite Observation, Copernicus Climate Change Service (C3S) Climate Data Store (CDS) [data set], https://doi.org/10.24381/cds.006f2c9a, 2019.

Denissen, J. M. C., Teuling, A. J., Pitman, A. J., Koirala, S., Migliavacca, M., Li, W., Reichstein, M., Winkler, A. J., Zhan, C., and Orth, R.: Widespread Shift from Ecosystem Energy to Water Limitation with Climate Change, Nat. Clim. Change, 12, 677–684, https://doi.org/10.1038/s41558-022-01403-8, 2022.

Didan, K. and Barreto Munoz, A.: MODIS vegetation index user's guide (MOD13 series), version 3.10, Vegetation Index and Phenology Lab, University of Arizona, 2019.

Donohue, R. J., Roderick, M. L., McVicar, T. R., and Farquhar, G. D.: Impact of CO_2 Fertilization on Maximum Foliage Cover across the Globe's Warm, Arid Environments: CO_2 FERTILIZATION AND FOLIAGE COVER, Geophys. Res. Lett., 40, 3031–3035, https://doi.org/10.1002/grl.50563, 2013.

https://doi.org/10.5194/egusphere-2026-5509
Preprint. Discussion started: 29 September 2026
© Author(s) 2026. CC BY 4.0 License.

Fan, L., Wigneron, J.-P., Ciais, P., Chave, J., Brandt, M., Sitch, S., Yue, C., Bastos, A., Li, X., Qin, Y., Yuan, W., Schepaschenko, D., Mukhortova, L., Li, X., Liu, X., Wang, M., Frappart, F., Xiao, X., Chen, J., Ma, M., Wen, J., Chen, X., Yang, H., van Wees, D., and Fensholt, R.: Siberian Carbon Sink Reduced by Forest Disturbances, Nat. Geosci., 16, 56–62, https://doi.org/10.1038/s41561-022-01087-x, 2023.

Feldman, A. F., Short Gianotti, D. J., Konings, A. G., McColl, K. A., Akbar, R., Salvucci, G. D., and Entekhabi, D.: Moisture Pulse-Reserve in the Soil-Plant Continuum Observed across Biomes, Nat. Plants, 4, 1026–1033, https://doi.org/10.1038/s41477-018-0304-9, 2018.

Feldman, A. F., Short Gianotti, D. J., Trigo, I. F., Salvucci, G. D., and Entekhabi, D.: Satellite-Based Assessment of Land Surface Energy Partitioning–Soil Moisture Relationships and Effects of Confounding Variables, Water Resour. Res., 55, 10657–10677, https://doi.org/10.1029/2019WR025874, 2019.

Feldman, A. F., Feng, X., Felton, A. J., Konings, A. G., Knapp, A. K., Biederman, J. A., and Poulter, B.: Plant Responses to Changing Rainfall Frequency and Intensity, Nat. Rev. Earth Environ., 5, 276–294, https://doi.org/10.1038/s43017-024-00534-0, 2024.

Feldman, A. F.: The Pulse of Global Vegetation: Do Individual Rainfall Events Create a Lasting Imprint on Photosynthesis?, New Phytol., 249, 736–743, https://doi.org/10.1111/nph.70463, 2026.

Feng, X., Fu, B., Zhang, Y., Pan, N., Zeng, Z., Tian, H., Lyu, Y., Chen, Y., Ciais, P., Wang, Y., Zhang, L., Cheng, L., Maestre, F. T., Fernández-Martínez, M., Sardans, J., and Peñuelas, J.: Recent leveling off of vegetation greenness and primary production reveals the increasing soil water limitations on the greening Earth, Sci. Bull., 66, 1462–1471, https://doi.org/10.1016/j.scib.2021.02.023, 2021.

Flach, M., Sippel, S., Gans, F., Bastos, A., Brenning, A., Reichstein, M., and Mahecha, M. D.: Contrasting Biosphere Responses to Hydrometeorological Extremes: Revisiting the 2010 Western Russian Heatwave, Biogeosciences, 15, 6067–6085, https://doi.org/10.5194/bg-15-6067-2018, 2018.

Frankenberg, C., Yin, Y., Byrne, B., He, L., and Gentine, P.: Comment on “Recent global decline of CO_2 fertilization effects on vegetation photosynthesis”, Science, 373, eabg2947, https://doi.org/10.1126/science.abg2947, 2021.

Fu, Z., Ciais, P., Feldman, A. F., Gentine, P., Makowski, D., Prentice, I. C., Stoy, P. C., Bastos, A., and Wigneron, J.-P.: Critical Soil Moisture Thresholds of Plant Water Stress in Terrestrial Ecosystems, Sci. Adv., 8, eabq7827, https://doi.org/10.1126/sciadv.abq7827, 2022.

Fu, Z., Ciais, P., Wigneron, J.-P., Gentine, P., Feldman, A. F., Makowski, D., Viovy, N., Kemanian, A. R., Goll, D. S., Stoy, P. C., Prentice, I. C., Yakir, D., Liu, L., Ma, H., Li, X., Huang, Y., Yu, K., Zhu, P., Li, X., Zhu, Z., Lian, J., and Smith, W. K.: Global Critical Soil Moisture Thresholds of Plant Water Stress, Nat. Commun., 15, 4826, https://doi.org/10.1038/s41467-024-49244-7, 2024.

Giardina, F., Gentine, P., Konings, A. G., Seneviratne, S. I., and Stocker, B. D.: Diagnosing Evapotranspiration Responses to Water Deficit across Biomes Using Deep Learning, New Phytol., 240, 968–983, https://doi.org/10.1111/nph.19197, 2023.

Huete, A., Didan, K., Miura, T., Rodriguez, E. P., Gao, X., and Ferreira, L. G.: Overview of the Radiometric and Biophysical Performance of the MODIS Vegetation Indices, Remote Sens. Environ., 83, 195–213, https://doi.org/10.1016/S0034-4257(02)00096-2, 2002.

Ingrisch, J. and Bahn, M.: Towards a Comparable Quantification of Resilience, Trends Ecol. Evol., 33, 251–259, https://doi.org/10.1016/j.tree.2018.01.013, 2018.

IPCC: Global Warming of 1.5 °C: An IPCC Special Report on the Impacts of Global Warming of 1.5 °C above Pre-industrial Levels and Related Global Greenhouse Gas Emission Pathways, in the Context of Strengthening the Global Response to the Threat of Climate Change, Sustainable Development, and Efforts to Eradicate

Poverty, edited by: Masson-Delmotte, V., Zhai, P., Pörtner, H.-O., Roberts, D., Skea, J., Shukla, P. R., Pirani, A., Moufouma-Okia, W., Péan, C., Pidcock, R., Connors, S., Matthews, J. B. R., Chen, Y., Zhou, X., Gomis, M. I., Lonnoy, E., Maycock, T., Tignor, M., and Waterfield, T., Intergovernmental Panel on Climate Change, Geneva, Switzerland, 2018.

IPCC: Climate Change and Land: An IPCC Special Report on Climate Change, Desertification, Land Degradation, Sustainable Land Management, Food Security, and Greenhouse Gas Fluxes in Terrestrial Ecosystems, edited by: Shukla, P. R., Skea, J., Calvo Buendia, E., Masson-Delmotte, V., Pörtner, H.-O., Roberts, D. C., Zhai, P., Slade, R., Connors, S., van Diemen, R., Ferrat, M., Haughey, E., Luz, S., Neogi, S., Pathak, M., Petzold, J., Portugal Pereira, J., Vyas, P., Huntley, E., Kissick, K., Belkacemi, M., and Malley, J., Intergovernmental Panel on Climate Change, Geneva, Switzerland, 2019.

IPCC: Climate Change 2021: The Physical Science Basis. Contribution of Working Group I to the Sixth Assessment Report of the Intergovernmental Panel on Climate Change, edited by: Masson-Delmotte, V., Zhai, P., Pirani, A., Connors, S. L., Péan, C., Berger, S., Caud, N., Chen, Y., Goldfarb, L., Gomis, M. I., Huang, M., Leitzell, K., Lonnoy, E., Matthews, J. B. R., Maycock, T. K., Waterfield, T., Yelekçi, O., Yu, R., and Zhou, B., Cambridge University Press, Cambridge, UK and New York, NY, USA, 2391 pp., https://doi.org/10.1017/9781009157896, 2021.

Jeong, S.-J., Ho, C.-H., Gim, H.-J., and Brown, M. E.: Phenology shifts at start vs. end of growing season in temperate vegetation over the Northern Hemisphere for the period 1982–2008, Glob. Change Biol., 17, 2385–2399, https://doi.org/10.1111/j.1365-2486.2011.02397.x, 2011.

Jeong, S.-J., Schimel, D., Frankenberg, C., Drewry, D. T., Fisher, J. B., Verma, M., Berry, J. A., Lee, J.-E., and Joiner, J.: Application of satellite solar-induced chlorophyll fluorescence to understanding large-scale variations in vegetation phenology and function over northern high latitude forests, Remote Sens. Environ., 190, 178–187, https://doi.org/10.1016/j.rse.2016.11.021, 2017.

Jeong, S., Ryu, Y., Gentine, P., Lian, X., Fang, J., Li, X., Dechant, B., Kong, J., Choi, W., Jiang, C., Keenan, T. F., Harrison, S. P., and Prentice, I. C.: Persistent global greening over the last four decades using novel long-term vegetation index data with enhanced temporal consistency, Remote Sens. Environ., 311, 114282, https://doi.org/10.1016/j.rse.2024.114282, 2024.

Jiao, W., Wang, L., Smith, W. K., Chang, Q., Wang, H., and D'Odorico, P.: Observed Increasing Water Constraint on Vegetation Growth over the Last Three Decades, Nat. Commun., 12, 3777, https://doi.org/10.1038/s41467-021-24016-9, 2021.

Jonard, F., Feldman, A. F., Short Gianotti, D. J., and Entekhabi, D.: Observed Water and Light Limitation across Global Ecosystems, Biogeosciences, 19, 5575–5590, https://doi.org/10.5194/bg-19-5575-2022, 2022.

Jump, A. S., Ruiz-Benito, P., Greenwood, S., Allen, C. D., Kitzberger, T., Fensham, R., Martínez-Vilalta, J., and Lloret, F.: Structural overshoot of tree growth with climate variability and the global spectrum of drought-induced forest dieback, Glob. Change Biol., 23, 3742–3757, https://doi.org/10.1111/gcb.13636, 2017.

Kannenberg, S. A., Schwalm, C. R., and Anderegg, W. R. L.: Ghosts of the Past: How Drought Legacy Effects Shape Forest Functioning and Carbon Cycling, Ecol. Lett., 23, 891–901, https://doi.org/10.1111/ele.13485, 2020.

Kendall, M. G.: Rank Correlation Methods, 4th edn., Charles Griffin, London, 1975.

Koppa, A., Rains, D., Hulsman, P., Poyatos, R., and Miralles, D. G.: A Deep Learning-Based Hybrid Model of Global Terrestrial Evaporation, Nat. Commun., 13, 1912, https://doi.org/10.1038/s41467-022-29543-7, 2022.

Kruskal, W. H. and Wallis, W. A.: Use of Ranks in One-Criterion Variance Analysis, J. Am. Stat. Assoc., 47, 583–621, https://doi.org/10.1080/01621459.1952.10483441, 1952.

https://doi.org/10.5194/egusphere-2026-5509
Preprint. Discussion started: 29 September 2026
© Author(s) 2026. CC BY 4.0 License.

Kühnhammer, K., van Haren, J., Kübert, A., Bailey, K., Dubbert, M., Hu, J., Ladd, S. N., Meredith, L. K., Werner, C., and Beyer, M.: Deep roots mitigate drought impacts on tropical trees despite limited quantitative contribution to transpiration, Sci. Total Environ., 893, 164763, https://doi.org/10.1016/j.scitotenv.2023.164763, 2023.

Lewis, S. L., Brando, P. M., Phillips, O. L., Van Der Heijden, G. M. F., and Nepstad, D.: The 2010 Amazon Drought, Science, 331, 554–554, https://doi.org/10.1126/science.1200807, 2011.

Lin, M., Lucas, H. C., and Shmueli, G.: Research Commentary —Too Big to Fail: Large Samples and the p-Value Problem, Inf. Syst. Res., 24, 906–917, https://doi.org/10.1287/isre.2013.0480, 2013.

Liu, Y., Li, Z., and Chen, Y.: Continuous warming shift greening towards browning in the Southeast and Northwest High Mountain Asia, Sci. Rep., 11, 17920, https://doi.org/10.1038/s41598-021-97240-4, 2021.

Liu, Q., Peng, C., Schneider, R., Cyr, D., Liu, Z., Zhou, X., Du, M., Li, P., Jiang, Z., McDowell, N. G., and Kneeshaw, D.: Vegetation browning: global drivers, impacts, and feedbacks, Trends Plant Sci., 28, 1014–1032, https://doi.org/10.1016/j.tplants.2023.03.024, 2023a.

Liu, X., Sun, G., Fu, Z., Ciais, P., Feng, X., Li, J., and Fu, B.: Compound droughts slow down the greening of the Earth, Glob. Change Biol., 29, 3072–3084, https://doi.org/10.1111/gcb.16657, 2023b.

Liu, Y., Li, Z., Chen, Y., Jin, L., Li, F., Wang, X., Long, Y., Liu, C., and Kayumba, P. M.: Global greening drives significant soil moisture loss, Commun. Earth Environ., 6, 600, https://doi.org/10.1038/s43247-025-02470-3, 2025.

Mann, H. B.: Nonparametric Tests Against Trend, Econometrica, 13, 245, https://doi.org/10.2307/1907187, 1945.

McColl, K. A., Wang, W., Peng, B., Akbar, R., Short Gianotti, D. J., Lu, H., Pan, M., and Entekhabi, D.: Global Characterization of Surface Soil Moisture Drydowns, Geophys. Res. Lett., 44, 3682–3690, https://doi.org/10.1002/2017GL072819, 2017.

McDowell, N., Pockman, W. T., Allen, C. D., Breshears, D. D., Cobb, N., Kolb, T., Plaut, J., Sperry, J., West, A., Williams, D. G., and Yepez, E. A.: Mechanisms of plant survival and mortality during drought: why do some plants survive while others succumb to drought?, New Phytol., 178, 719–739, https://doi.org/10.1111/j.1469-8137.2008.02436.x, 2008.

McDowell, N. G., Anderson-Teixeira, K., Biederman, J. A., Breshears, D. D., Fang, Y., Fernández-de-Uña, L., Graham, E. B., Mackay, D. S., McDonnell, J. J., Moore, G. W., Nehemy, M. F., Stevens Rumann, C. S., Stegen, J., Tague, N., Turner, M. G., and Chen, X.: Ecohydrological Decoupling under Changing Disturbances and Climate, One Earth, 6, 251–266, https://doi.org/10.1016/j.oneear.2023.02.007, 2023.

McLeod, A. I.: Kendall: Kendall Rank Correlation and Mann-Kendall Trend Test, October 28, https://doi.org/10.32614/CRAN.package.Kendall, 2005.

Miller, D. L., Wolf, S., Fisher, J. B., Zaitchik, B. F., Xiao, J., and Keenan, T. F.: Increased photosynthesis during spring drought in energy-limited ecosystems, Nat. Commun., 14, 7828, https://doi.org/10.1038/s41467-023-43430-9, 2023.

Miralles, D. G., Holmes, T. R. H., De Jeu, R. A. M., Gash, J. H., Meesters, A. G. C. A., and Dolman, A. J.: Global land-surface evaporation estimated from satellite-based observations, Hydrol. Earth Syst. Sci., 15, 453–469, https://doi.org/10.5194/hess-15-453-2011, 2011.

Miralles, D. G., Bonte, O., Koppa, A., Baez-Villanueva, O. M., Tronquo, E., Zhong, F., Beck, H. E., Hulsman, P., Dorigo, W., Verhoest, N. E. C., and Haghdoost, S.: GLEAM4: Global Land Evaporation and Soil Moisture Dataset at 0.1° Resolution from 1980 to near Present, Sci. Data, 12, 416, https://doi.org/10.1038/s41597-025-04610-y, 2025a.

Miralles, D. G., Vilà-Guerau de Arellano, J., and Mahecha, M. D.: Vegetation–climate feedbacks across scales,

https://doi.org/10.5194/egusphere-2026-5509
Preprint. Discussion started: 29 September 2026
© Author(s) 2026. CC BY 4.0 License.

Ann. N. Y. Acad. Sci., 1544, 27–41, https://doi.org/10.1111/nyas.15286, 2025b.

Nakagawa, S. and Cuthill, I. C.: Effect Size, Confidence Interval and Statistical Significance: A Practical Guide for Biologists, Biol. Rev., 82, 591–605, https://doi.org/10.1111/j.1469-185X.2007.00027.x, 2007.

Nemani, R. R., Keeling, C. D., Hashimoto, H., Jolly, W. M., Piper, S. C., Tucker, C. J., Myneni, R. B., and Running, S. W.: Climate-Driven Increases in Global Terrestrial Net Primary Production from 1982 to 1999, Science, 300, 1560–1563, https://doi.org/10.1126/science.1082750, 2003.

Novick, K. A., Ficklin, D. L., Stoy, P. C., Williams, C. A., Bohrer, G., Oishi, A. C., Papuga, S. A., Blanken, P. D., Noormets, A., Sulman, B. N., Scott, R. L., Wang, L., and Phillips, R. P.: The increasing importance of atmospheric demand for ecosystem water and carbon fluxes, Nat. Clim. Change, 6, 1023–1027, https://doi.org/10.1038/nclimate3114, 2016.

Orth, R., Zscheischler, J., and Seneviratne, S. I.: Record Dry Summer in 2015 Challenges Precipitation Projections in Central Europe, Sci. Rep., 6, 28334, https://doi.org/10.1038/srep28334, 2016.

Orth, R., Denissen, J. M. C., Kroll, J., O, S., Bastos, A., Li, W., Miralles, D. G., Ruiz-Vásquez, M., Hoek van Dijke, A. J., Feldman, A. F., Migliavacca, M., Wang-Erlandsson, L., Stocker, B. D., Teuling, A. J., Yang, H., Zhan, C., and Yu, X.: Regional Emergence of Water-Related Browning in a Greening World, Glob. Change Biol., 31, e70620, https://doi.org/10.1111/gcb.70620, 2025.

Pan, N., Feng, X., Fu, B., Wang, S., Ji, F., and Pan, S.: Increasing Global Vegetation Browning Hidden in Overall Vegetation Greening: Insights from Time-Varying Trends, Remote Sens. Environ., 214, 59–72, https://doi.org/10.1016/j.rse.2018.05.018, 2018.

Penman, H. L.: Natural Evaporation from Open Water, Bare Soil and Grass, Proc. R. Soc. Lond. A, 193, 120–145, https://doi.org/10.1098/rspa.1948.0037, 1948.

Piao, S., Liu, Q., Chen, A., Janssens, I. A., Fu, Y., Dai, J., Liu, L., Lian, X., Shen, M., and Zhu, X.: Plant Phenology and Global Climate Change: Current Progresses and Challenges, Glob. Change Biol., 25, 1922–1940, https://doi.org/10.1111/gcb.14619, 2019.

Pohlert, T.: Trend: Non-Parametric Trend Tests and Change-Point Detection, March 24, https://doi.org/10.32614/CRAN.package.trend, 2015.

Romano, J., Kromrey, J. D., Coraggio, J., and Skowronek, J.: Appropriate statistics for ordinal level data: should we really be using t-test and Cohen's d for evaluating group differences on the NSSE and other surveys?, Annual Meeting of the Florida Association of Institutional Research, 2006.

Schwalm, C. R., Anderegg, W. R. L., Michalak, A. M., Fisher, J. B., Biondi, F., Koch, G., Litvak, M., Ogle, K., Shaw, J. D., Wolf, A., Huntzinger, D. N., Schaefer, K., Cook, R., Wei, Y., Fang, Y., Hayes, D., Huang, M., Jain, A., and Tian, H.: Global Patterns of Drought Recovery, Nature, 548, 202–205, https://doi.org/10.1038/nature23021, 2017.

Seddon, A. W. R., Macias-Fauria, M., Long, P. R., Benz, D., and Willis, K. J.: Sensitivity of global terrestrial ecosystems to climate variability, Nature, 531, 229–232, https://doi.org/10.1038/nature16986, 2016.

Seneviratne, S. I., Corti, T., Davin, E. L., Hirschi, M., Jaeger, E. B., Lehner, I., Orlowsky, B., and Teuling, A. J.: Investigating Soil Moisture–Climate Interactions in a Changing Climate: A Review, Earth-Sci. Rev., 99, 125–161, https://doi.org/10.1016/j.earscirev.2010.02.004, 2010.

Slette, I. J., Post, A. K., Awad, M., Even, T., Punzalan, A., Williams, S., Smith, M. D., and Knapp, A. K.: How Ecologists Define Drought, and Why We Should Do Better, Glob. Change Biol., 25, 3193–3200, https://doi.org/10.1111/gcb.14747, 2019.

Spracklen, D. V., Baker, J. C. A., Garcia-Carreras, L., and Marsham, J. H.: The Effects of Tropical Vegetation on Rainfall, Annu. Rev. Environ. Resour., 43, 193–218, https://doi.org/10.1146/annurev-environ-102017-030136,

https://doi.org/10.5194/egusphere-2026-5509
Preprint. Discussion started: 29 September 2026
© Author(s) 2026. CC BY 4.0 License.

2018.

Stocker, B. D., Tumber-Dávila, S. J., Konings, A. G., Anderson, M. C., Hain, C., and Jackson, R. B.: Global patterns of water storage in the rooting zones of vegetation, Nat. Geosci., 16, 250–256, https://doi.org/10.1038/s41561-023-01125-2, 2023.

Tomczak, M. and Tomczak, E.: The need to report effect size estimates revisited. An overview of some recommended measures of effect size, Trends Sport Sci., 21, 19–25, 2014.

Turner, M. G. and Seidl, R.: Novel Disturbance Regimes and Ecological Responses, Annu. Rev. Ecol. Evol. Syst., 54, 63–83, https://doi.org/10.1146/annurev-ecolsys-110421-101120, 2023.

van der Sleen, P., Groenendijk, P., Vlam, M., Anten, N. P. R., Boom, A., Bongers, F., Pons, T. L., Terburg, G., and Zuidema, P. A.: No growth stimulation of tropical trees by 150 years of CO_2 fertilization but water-use efficiency increased, Nat. Geosci., 8, 24–28, https://doi.org/10.1038/ngeo2313, 2015.

Van Loon, A. F., Kchouk, S., Matanó, A., Tootoonchi, F., Alvarez-Garreton, C., Hassaballah, K. E. A., Wu, M., Wens, M. L. K., Shyrokaya, A., Ridolfi, E., Biella, R., Nagavciuc, V., Barendrecht, M. H., Bastos, A., Cavalcante, L., de Vries, F. T., Garcia, M., Mård, J., Streefkerk, I. N., Teutschbein, C., Tootoonchi, R., Weesie, R., Aich, V., Boisier, J. P., Di Baldassarre, G., Du, Y., Galleguillos, M., Garreaud, R., Ionita, M., Khatami, S., Koehler, J. K. L., Luce, C. H., Maskey, S., Mendoza, H. D., Mwangi, M. N., Pechlivanidis, I. G., Ribeiro Neto, G. G., Roy, T., Stefanski, R., Trambauer, P., Koebele, E. A., Vico, G., and Werner, M.: Review article: Drought as a continuum – memory effects in interlinked hydrological, ecological, and social systems, Nat. Hazards Earth Syst. Sci., 24, 3173–3205, https://doi.org/10.5194/nhess-24-3173-2024, 2024.

Venables, W. N. and Ripley, B. D.: Modern Applied Statistics with S, 4th edn., Statistics and Computing, Springer, New York, 2002.

Vicente-Serrano, S. M., Gouveia, C., Camarero, J. J., Beguería, S., Trigo, R., López-Moreno, J. I., Azorín-Molina, C., Pasho, E., Lorenzo-Lacruz, J., Revuelto, J., Morán-Tejeda, E., and Sanchez-Lorenzo, A.: Response of vegetation to drought time-scales across global land biomes, Proc. Natl. Acad. Sci. USA, 110, 52–57, https://doi.org/10.1073/pnas.1207068110, 2013.

Walther, S., Voigt, M., Thum, T., Gonsamo, A., Zhang, Y., Köhler, P., Jung, M., Varlagin, A., and Guanter, L.: Satellite chlorophyll fluorescence measurements reveal large-scale decoupling of photosynthesis and greenness dynamics in boreal evergreen forests, Glob. Change Biol., 22, 2979–2996, https://doi.org/10.1111/gcb.13200, 2016.

Wang, C., Chen, J., Wu, J., Tang, Y., Shi, P., Black, T. A., and Zhu, K.: A snow-free vegetation index for improved monitoring of vegetation spring green-up date in deciduous ecosystems, Remote Sens. Environ., 196, 1–12, https://doi.org/10.1016/j.rse.2017.04.031, 2017.

Webb, E. E., Alexander, H. D., Paulson, A. K., Loranty, M. M., DeMarco, J., Talucci, A. C., Spektor, V., Zimov, N., and Lichstein, J. W.: Fire-Induced Carbon Loss and Tree Mortality in Siberian Larch Forests, Geophys. Res. Lett., 51, e2023GL105216, https://doi.org/10.1029/2023GL105216, 2024.

Wolf, S., Keenan, T. F., Fisher, J. B., Baldocchi, D. D., Desai, A. R., Richardson, A. D., Scott, R. L., Law, B. E., Litvak, M. E., Brunsell, N. A., Peters, W., and van der Laan-Luijkx, I. T.: Warm Spring Reduced Carbon Cycle Impact of the 2012 US Summer Drought, Proc. Natl. Acad. Sci. USA, 113, 5880–5885, https://doi.org/10.1073/pnas.1519620113, 2016.

Xiao, C., Zaehle, S., Sitch, S., Duveiller, G., Pabon-Moreno, D. E., Walker, A. P., Knauer, J., Maignan, F., Schmullius, C., and Bastos, A.: Deforestation increases vegetation vulnerability to drought across biomes, ESS Open Archive [preprint], https://doi.org/10.22541/essoar.172901224.44997446/v1, 2024.

Xu, L., Samanta, A., Costa, M. H., Ganguly, S., Nemani, R. R., and Myneni, R. B.: Widespread decline in

https://doi.org/10.5194/egusphere-2026-5509
Preprint. Discussion started: 29 September 2026
© Author(s) 2026. CC BY 4.0 License.

greenness of Amazonian vegetation due to the 2010 drought, Geophys. Res. Lett., 38, L07402, https://doi.org/10.1029/2011GL046824, 2011.

Yang, Y., Roderick, M. L., Guo, H., Miralles, D. G., Zhang, L., Fatichi, S., Luo, X., Zhang, Y., McVicar, T. R., Tu, Z., Keenan, T. F., Fisher, J. B., Gan, R., Zhang, X., Piao, S., Zhang, B., and Yang, D.: Evapotranspiration on a Greening Earth, Nat. Rev. Earth Environ., 4, 626–641, https://doi.org/10.1038/s43017-023-00464-3, 2023.

Zeng, Z., Piao, S., Li, L. Z. X., Wang, T., Ciais, P., Lian, X., Yang, Y., Mao, J., Shi, X., and Myneni, R. B.: Impact of Earth Greening on the Terrestrial Water Cycle, J. Climate, 31, 2633–2650, https://doi.org/10.1175/JCLI-D-17-0236.1, 2018.

Zhang, Y., Song, C., Band, L. E., Sun, G., and Li, J.: Reanalysis of global terrestrial vegetation trends from MODIS products: Browning or greening?, Remote Sens. Environ., 191, 145–155, https://doi.org/10.1016/j.rse.2016.12.018, 2017.

Zhang, Y., Keenan, T. F., and Zhou, S.: Exacerbated drought impacts on global ecosystems due to structural overshoot, Nat. Ecol. Evol., 5, 1490–1498, https://doi.org/10.1038/s41559-021-01551-8, 2021.

Zhou, S., Williams, A. P., Berg, A. M., Cook, B. I., Zhang, Y., Hagemann, S., Lorenz, R., Seneviratne, S. I., and Gentine, P.: Land–atmosphere feedbacks exacerbate concurrent soil drought and atmospheric aridity, Proc. Natl. Acad. Sci. USA, 116, 18848–18853, https://doi.org/10.1073/pnas.1904955116, 2019.

Zhu, Z., Piao, S., Myneni, R. B., Huang, M., Zeng, Z., Canadell, J. G., Ciais, P., Sitch, S., Friedlingstein, P., Arneth, A., Cao, C., Cheng, L., Kato, E., Koven, C., Li, Y., Lian, X., Liu, Y., Liu, R., Mao, J., Pan, Y., Peng, S., Peñuelas, J., Poulter, B., Pugh, T. A. M., Stocker, B. D., Viovy, N., Wang, X., Wang, Y., Xiao, Z., Yang, H., Zaehle, S., and Zeng, N.: Greening of the Earth and Its Drivers, Nat. Clim. Change, 6, 791–795, https://doi.org/10.1038/nclimate3004, 2016.